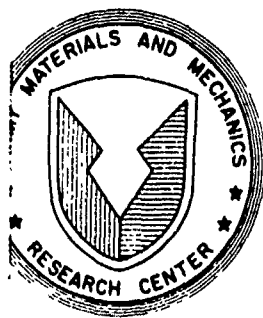ADA048076

AMMRC CTR 77-24

STRUCTURAL ANALYSIS AND TESTING FOR COMPOSITE FLYWHEEL DEVELOPMENT.

SEP 77

68 p.

DONALD E. JOHNSON

AVCO SYSTEMS DIVISION
201 LOWELL ST., WILMINGTON, MA 01887

Final Report Contract Number DAAG46-77-C-0017

24 Jan - 3 Sep 77,

Approved for public release; distribution unlimited.

Prepared for

ARMY MATERIALS AND MECHANICS RESEARCH CENTER
Watertown, Massachusetts 02172

AD

D D C

JAN 4 1978

B

The findings in this report are not to be construed as an official
Department of the Army position, unless so designated by other
authorized documents.

Mention of any trade names or manufacturers in this report
shall not be construed as advertising nor as an official
indorsement or approval of such products or companies by
the United States Government.

REPORT DOCUMENTATION PAGE		READ INSTRUCTIONS BEFORE COMPLETING FORM
1 REPORT NUMBER AMMRC CTR 77-24	2 GOVT ACCESSION NO.	3 RECIPIENT'S CATALOG NUMBER
4 TITLE (and Subtitle) STRUCTURAL ANALYSIS AND TESTING FOR COMPOSITE FLYWHEEL DEVELOPMENT		5 TYPE OF REPORT & PERIOD COVERED FINAL REPORT 1/24/77 - 9/3/77
		6 PERFORMING ORG. REPORT NUMBER
7 AUTHOR(s) Donald E. Johnson		8 CONTRACT OR GRANT NUMBER(s) *NEW* DAAG46-77-C-0017
9 PERFORMING ORGANIZATION NAME AND ADDRESS Avco Systems Division 201 Lowell Street Wilmington, Massachusetts 01887		10 PROGRAM ELEMENT, PROJECT, TASK AREA & WORK UNIT NUMBERS D/A Project: AMCMS Code: Agency Accession:
11. CONTROLLING OFFICE NAME AND ADDRESS Army Materials and Mechanics Research Center Watertown, Massachusetts 02172		12 REPORT DATE September 1977
		13 NUMBER OF PAGES
14 MONITORING AGENCY NAME & ADDRESS(if different from Controlling Office)		15 SECURITY CLASS (of this report) Unclassified
		15a DECLASSIFICATION/DOWNGRADING SCHEDULE

16. DISTRIBUTION STATEMENT (of this Report)

Approved for public release; distribution unlimited.

17. DISTRIBUTION STATEMENT (of the abstract entered in Block 20, if different from Report)

DDC

RECEIVED
JAN 4 1978
RECEIVED

B

18 SUPPLEMENTARY NOTES

19 KEY WORDS (Continue on reverse side if necessary and identify by block number)

Flywheels	Fracture
Composite materials	Stress analysis
Failure	

20 ABSTRACT (Continue on reverse side if necessary and identify by block number)

(SEE REVERSE SIDE)

Block No. 20

ABSTRACT

Several effects that can limit the performance of bi-directionally reinforced composite flywheels are investigated. These effects include potential shear failures, degraded properties and variations caused by manufacturing. Finite element analyses are used to determine both the in-plane and interlaminar shear stresses that arise from the discreteness of the individual radial reinforcements. The degradation of material properties due to high biaxial stress levels, especially a drop in shear modulus, is also investigated. Degraded properties are obtained experimentally and used in the evaluation of flywheel performance. Also included is an analysis to determine the feasibility of a static simulation test. In addition, the effect of asymmetric material property variation on flywheel imbalance was investigated.

ACCESSION for

NTIS	White Section	☑
DDC	Buff Section	☐
UNANNOUNCED		☐
JUSTIFICATION		

BY
DISTRIBUTION/AVAILABILITY CODES

Dist.	AVAIL and/or SPECIAL	
A		

CONTENTS

ILLUSTRATIONS

FOREWORD

SECTION 1

INTRODUCTION

1.1 SUMMARY

This report summarizes the results of an investigation of bi-directionally reinforced composite flywheels. The investigation focuses on the hoop-radial type of bi-directional configuration developed by Avco and includes both analytical and experimental work. This work is divided into four major portions:

- Analytical Assessment of the Effect of Degraded Material Properties (Section 2)

- Sensitivity Studies (Section 3)

- Analysis of Static Simulation Test (Section 4)

- Testing for Degraded Property Effects (Section 5)

Some conclusions from this work are: (1) decreases of in-plane shear modulus of up to 90 percent have small effect on the maximum stresses, (2) changes in hoop thickness or fiber volume ratio can cause changes of similar magnitude in theoretical flywheel efficiency, (3) static simulation tests are feasible but must include substantial numbers of radials to prevent premature shear failures, and (4) degraded property effects can be measured experimentally and substantial reductions in moduli and shear stress allowables are found. These and other results are discussed in greater detail in Section 6.

1.2 BACKGROUND AND PRELIMINARY DEVELOPMENT

Bi-directionally reinforced flywheels offer potential advantages over the more conventional composite ring designs, such as greater energy per unit volume and a larger number of geometric parameters to apply to the design of hub connections. In addition, theoretical analyses show that the stored kinetic energy per unit weight of a bi-directionally reinforced wheel can be within a few percent of that obtained through ring designs.

The kinetic energy per unit weight of a composite flywheel composed of one material can be written in the following form.

$$\frac{\text{Kinetic Energy}}{\text{Weight}} = K_s \frac{\sigma}{\rho g}$$

where

K_s = shape factor

σ = allowable tensile stress of a 1-D ply in the 0° direction

ρg = weight/unit volume of the wheel.

For a given material σ and ρg are known and the primary problem is to configure the wheel to achieve the highest possible value of K_s. Analyses[*] based on the neglecting of the very low 90° tensile strengths indicate that the maximum K_s obtainable for a composite is .5. (For a simple ring K_s = .5.) Design experience at Avco indicates that some deviation from the optimum is necessary to prevent excessive hoop-radial interlaminar shear stresses. As a result the shape factor K_s must be slightly reduced from .5 to .474. It should be noted that since the formula for kinetic energy per unit weight involves only the strength in the 0° direction, the formula applies to a flywheel which has been designed to avoid premature failures associated with other stress components.

The Avco bi-directional flywheel design consists of a stacked sequence of hoop and radial layers. The hoop layers are approximately .017-inch thick and essentially axisymmetric. The radial layers each contain 144 radial members .008-inch thick and of tapered width to provide optimum efficiency. The material is Kevlar 49. A simplified schematic drawing of the Avco design is shown in Figure 1-1. This schematic drawing shows only 16 of the 144 radial members present in the actual design. This design[**] is used as a reference point for the investigations carried out for this report. Consequently, it is appropriate to outline and define the basic parameters that controlled the reference design.

At the onset we introduce appropriate nondimensional stress nomenclature as follows:

$$\hat{\sigma} = \frac{\sigma}{\rho \Omega^2 R^2}$$

where

σ = stress

$\hat{\sigma}$ = nondimensional stress

ρ = mass density of a ply

[*]Johnson, D. E., Maximum Shape Factor for Composite Flywheel Avco Technical Release K400-T-322-A, August 27, 1975.

[**]Sapowith, A., Phase I Interim Technical Report, Avco AVSD-0189-76-CR, June 18, 1976.
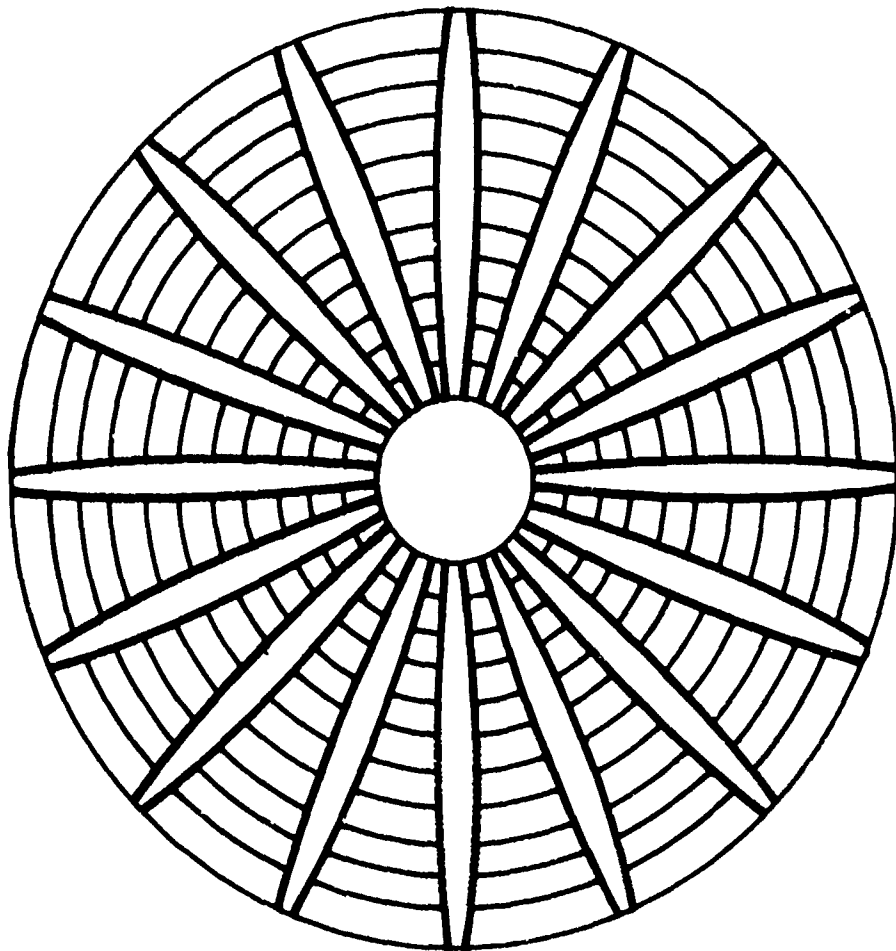
85-1569

Figure 1—1. Schematic of typical bi-directionally reinforced flywheel.

Ω = angular velocity in radians/sec.

R = outside radius of the flywheel

The nondimensionalization symbol ^ is applied to various stress components. The nondimensional aspect of this problem implies that the results from these analyses can be applied to a whole family of wheels of varying outside radius -- provided the thicknesses of the individual plys are scaled proportionately with the outside radius.

The dominant feature of an efficient bi-directional flywheel is a biaxial state of stress with approximately equal stresses in the hoop and radial directions. For Kevlar the 0° and 90° failure strains, ϵ_0 and ϵ_{90} form the following ratio

$$\frac{\epsilon_{90}}{\epsilon_0} = \frac{0.22\%}{1.6\%} = .138$$

This implies that the transverse (90°) properties of the Kevlar will be degraded, and crazing will occur well before the 0° failure strains are reached. Because of this reason the radial configuration for the reference Kevlar flywheel was designed on the basis of $E_{90} = 0$ in each hoop and radial ply. To implement the iterations required during the design process a "smeared out" axisymmetric finite element model was used to obtain the optimally shaped radial reinforcements that yielded the highest shape factor K_s. The nondimensional stresses derived from the axisymmetric model are shown in Figure 1-2. This figure clearly shows the dominant features of the problem: nearly biaxial ($\sigma_r = \sigma_\theta$) stresses over the interior of the wheel and very much smaller shear stresses σ_{rz} and $\sigma_{r\theta}$ (see separate scale on right side of the figure). Unfortunately the shear allowables are correspondingly smaller, as may be seen from Table 1-1 which summarizes the maxima of the stresses shown in Figure 1-2 together with the corresponding stresses from a more complex two-dimensional finite element model of the same problem. The 2-D model is thus used as a check on the simpler equivalent axisymmetric model which is so well suited for the parametric variations of radial geometry required during design.

TABLE 1-1. STRESSES IN REFERENCE FLYWHEEL DESIGN
FOR $E_{90} = 0$ (DEGRADED)

Type of Stress	Equivalent axisymmetric analysis		2-D Finite element		Allowables*
	Nondimensional	At Ω = 5685 radians/sec	Nondimensional	At Ω = 5630 radians/sec	
σ_r	.516	200 ksi	.514	200 ksi	188-211 ksi
σ_θ	.516	200 ksi	.530	200 ksi	188-211 ksi
σ_{rz}	.00401	1.55 ksi	.00355	1.34 ksi	1.45-7.9 ksi
$\sigma_{r\theta}$	.00982	3.81 ksi	.01032	3.90 ksi	7.9 ksi

*Based on Avco tests and duPont report "Characteristics and Uses of Kevlar 49 High Modulus Organic Fiber," by R. L. Hunter, revised 9/18/73.
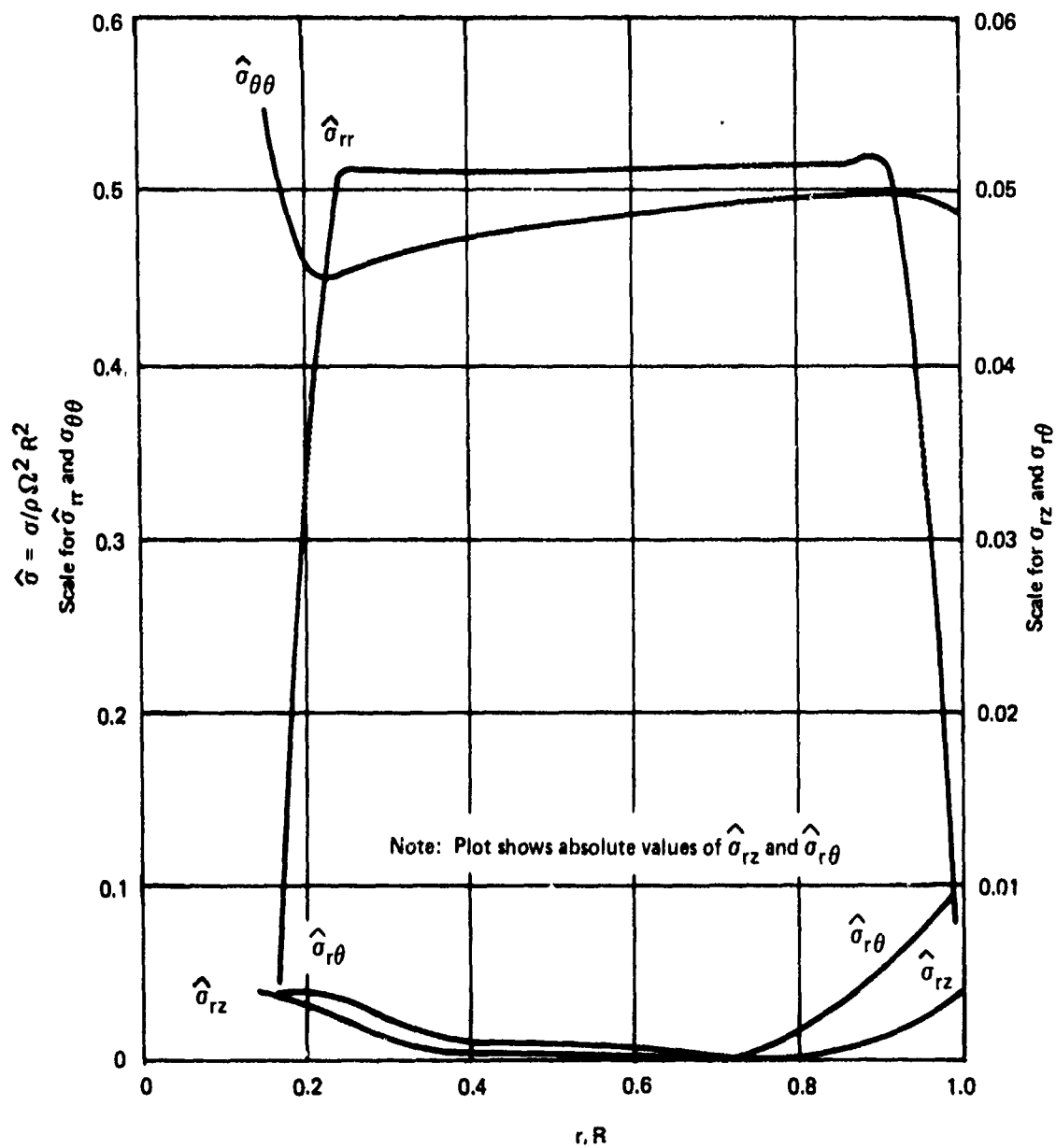
97-700

Figure 1–2. Non-dimensional stresses from equivalent axisymmetric model – – reference design.

Material Properties

Unless otherwise specified, the following Kevlar 49 mechanical properties are used in this report:

Property	Equivalent nomenclature	Values used	
		Undegraded	Degraded
E_1	$E_0 = E$	12×10^6 psi	12×10^6 psi
$E_2 = E_3$	E_{90}	0.8×10^6	0
$\nu_{12} = \nu_{13}$		.34	0
$\nu_{21} = \nu_{31}$		.0227	0
ν_{32}		.48	0
G_{12}	G	0.3×10^6 psi	$.3 \times 10^6$ psi or reduced*

These properties are derived from the properties given by duPont.** As pointed out in the previous section the degraded properties were used in the flywheel design because of the very low transverse (90°) strain capability of Kevlar. It should also be noted that the linear elastic nature of the problem is such that the resulting stresses are unchanged if the moduli E_1, E_2, E_3 and G are multiplied by the same scalar constant.

Comparison of Finite Element Models

Three different types of finite element models were used in this report:

1. 1-D Axisymmetric Model

2. 2-D Model including Discrete Radials

3. 2-D Model using "Smeared Out" Properties

Each of these three models assumes plane stress. Solutions from the 1-D axisymmetric model are functions of the radial coordinate, r, only. Solutions of the 2-D models are functions of both r and θ.

Examples of the finite element grids used in these three models are shown in Figures 1-3 through 1-5. In the 2-D model with discrete radials shown in Figure 1-4, the nodes in the hoop-radial overlap region each have one set of planar displacements, i.e., in spite of the overlapping the model remains

---

*An investigation in which G_{12} is reduced below this value is presented in Section 2 of this report.
**Hunter, R. L., "Characteristics and Uses of Kevlar 49 High Modulus Organic Fiber," duPont Report, revised 9/18/73.
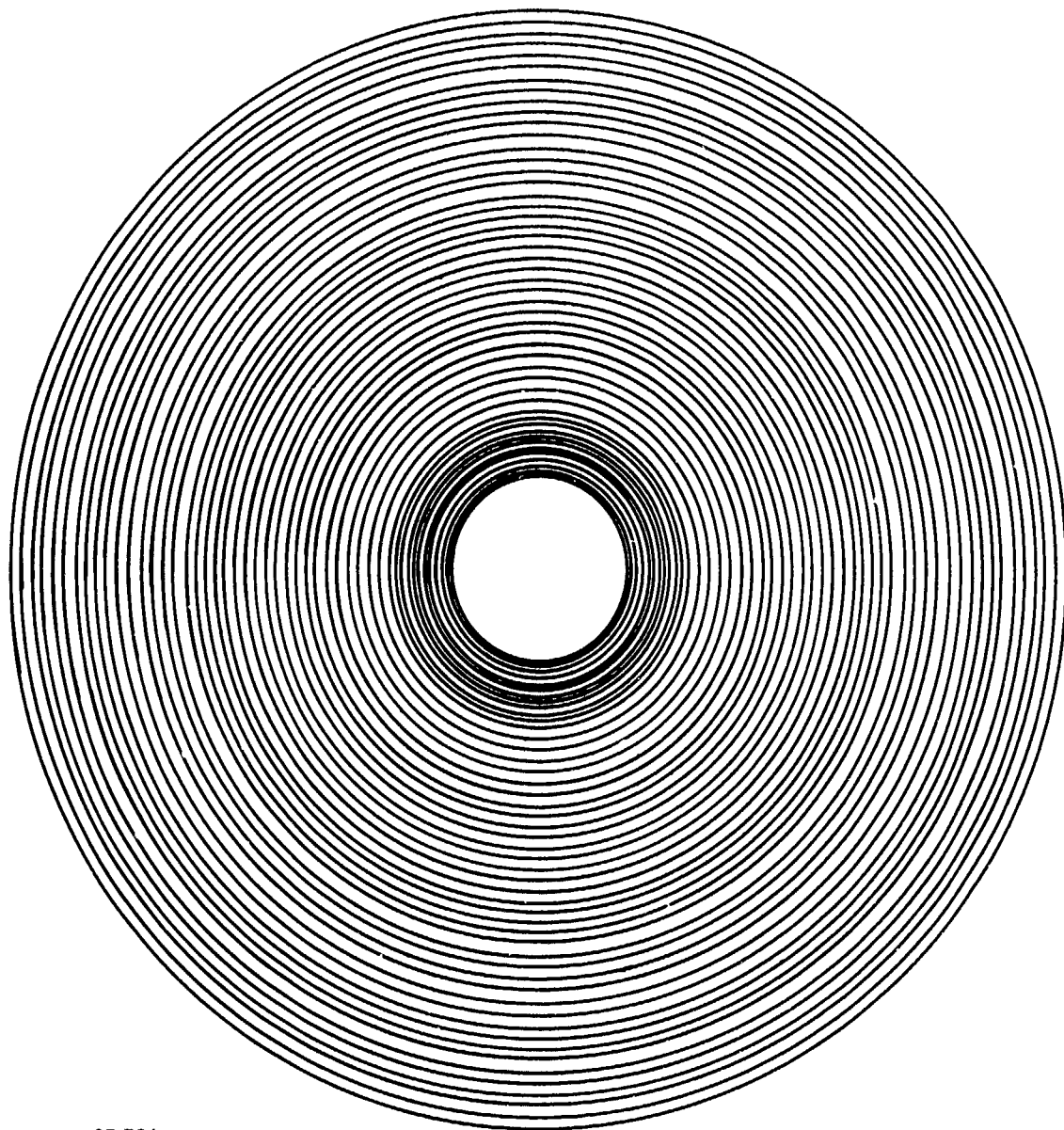
97-701

Figure 1—3. One dimensional finite element grid used for axisymmetric analyses.

Radial over Hoop

Hoop only

r = 1.625″

2.8

4.5

7.2

9.75

1.25° sector

97-702

Local radius, inches
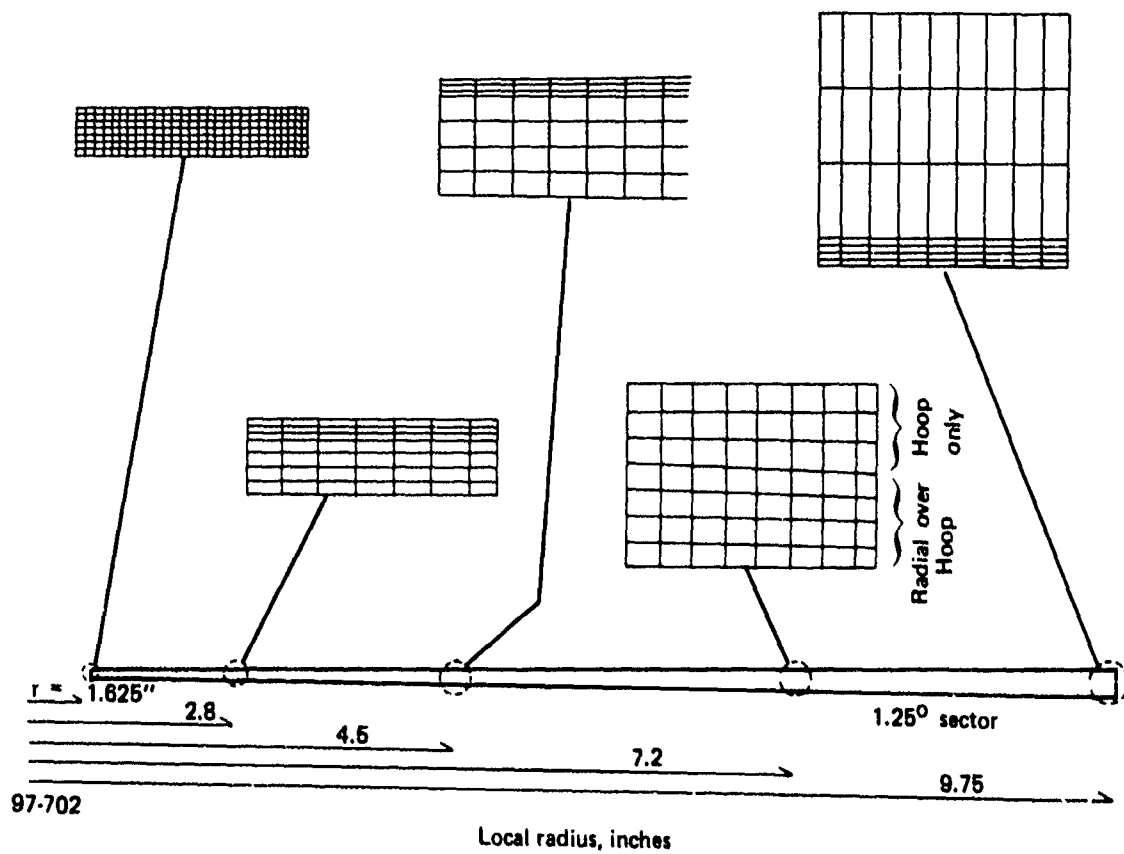
Figure 1—4. Samples of 2-D finite element mesh at various radii.
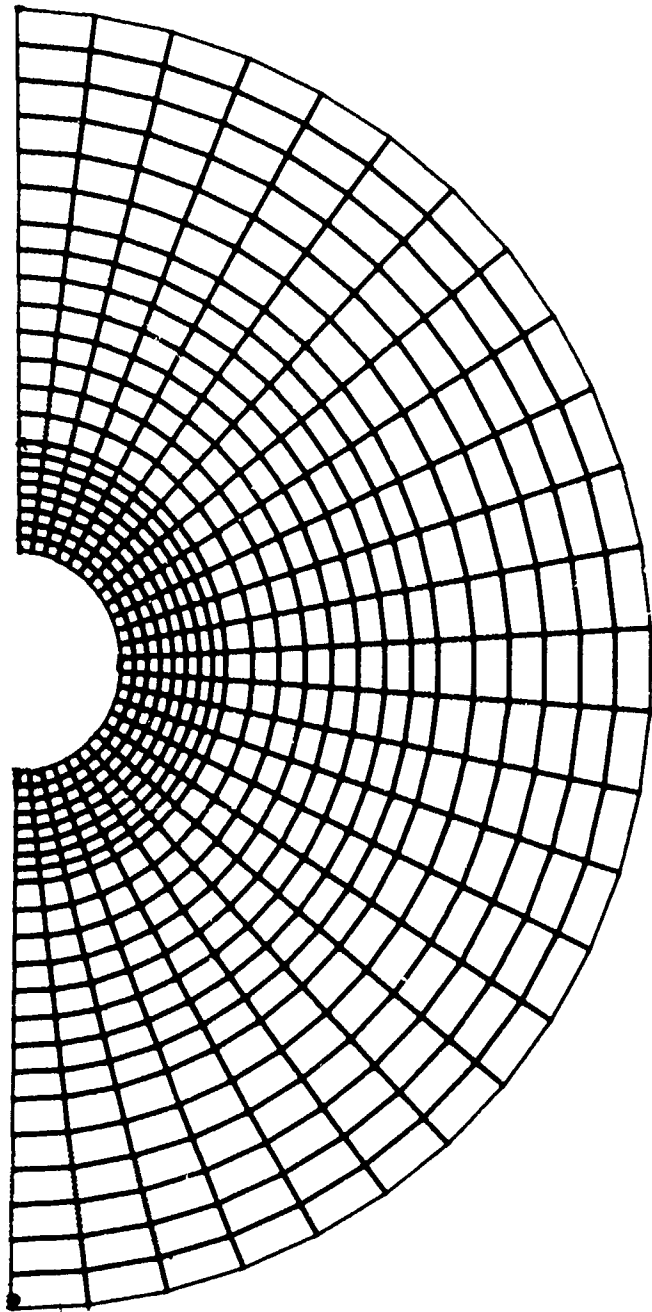
97-703

Figure 1–5. Finite element grid used for asymmetric property variations.

planar. This model uses 2488 nodes and 3410 elements to represent the very slender angular section shown in Figure 1-4.

Most of the work was done using the first two models, the last being mainly used to determine the effects of gross asymmetries and imbalance.

Each of the three finite element models produces the σ_{rr} stresses in the radials and the $\sigma_{\theta\theta}$ stresses in the hoops directly. In the 2-D models the in-plane shear stresses $\sigma_{r\theta}$ are also produced directly. Because of the axisymmetry of the 1-D finite element model, it gives $\sigma_{r\theta} = \sigma_{r\theta} = 0$. Nevertheless, it is possible to start with the $\sigma_{\theta\theta}$ from the 1-D model and compute, via static equilibrium, the $\sigma_{r\theta}$ stresses that would occur if one had a set of discrete radial reinforcements as shown in Figure 1-1. The essence of this calculation is shown in Figure 4-5 and is based on the previously cited damaged properties. None of the three finite element models used in this work gives the interlaminar stress σ_{rz} directly. Consequently, the σ_{rz} stresses were obtained from the other stresses by using static equilibrium. The method applied to the 1-D model is very similar to that used for obtaining $\sigma_{r\theta}$ and is outlined in Figure 4-5. The stresses σ_{rz} for the 2-D model were also derived using static equilibrium: In this case the net force on a small element of each layer (hoop and radial) were computed and used to determine the force transferred between the layers by the interlaminar shear stress.

Because the state of stress in the bi-directionally reinforced wheel is almost axisymmetric, the stress distributions presented in this report are generally plotted as functions of the radial coordinate r. The relatively small deviations from axisymmetry, when they appear, are indicated by showing the maximum and minimum values with respect to changes in the θ (circumferential) coordinate. In figures such as 1-8 or 2-3, the deviation from axisymmetry is sufficiently great so that two separate dashed curves are used to show the maximum and minimum values.

Because these several different models were used to carry out the work presented in this report, it is appropriate to pause and obtain a check of the accuracy by comparing results obtained by the different models for the original flywheel design. This was carried out for two different cases, one using the undegraded properties shown in the table and one using the degraded properties (with $G = .3 \times 10^6$).

Figures 1-6 through 1-9 show that for the hoop and radial stresses the two models give almost the same results for each case. the difference between them being of the same order as the circumferential variation (see $\sigma_{\theta\theta}$) within the 2-D model itself. Similar agreement is seen in Figure 1-10 for the $\sigma_{r\theta}$ shear stresses. The σ_{rz} stresses shown in Figure 1-11, however, show a considerable difference between the average σ_{rz} values derived from the axisymmetric model and those from the 2-D model. This latter difference is not accountable from the circumferential variations in the 2-D model but appears to be caused by a fundamental difference between the two models. Because of the planar nature of the 2-D model it gives a $\sigma_{r\theta}$ that does not approach zero at the edge of a radial. This can violate the shear-free condition actually
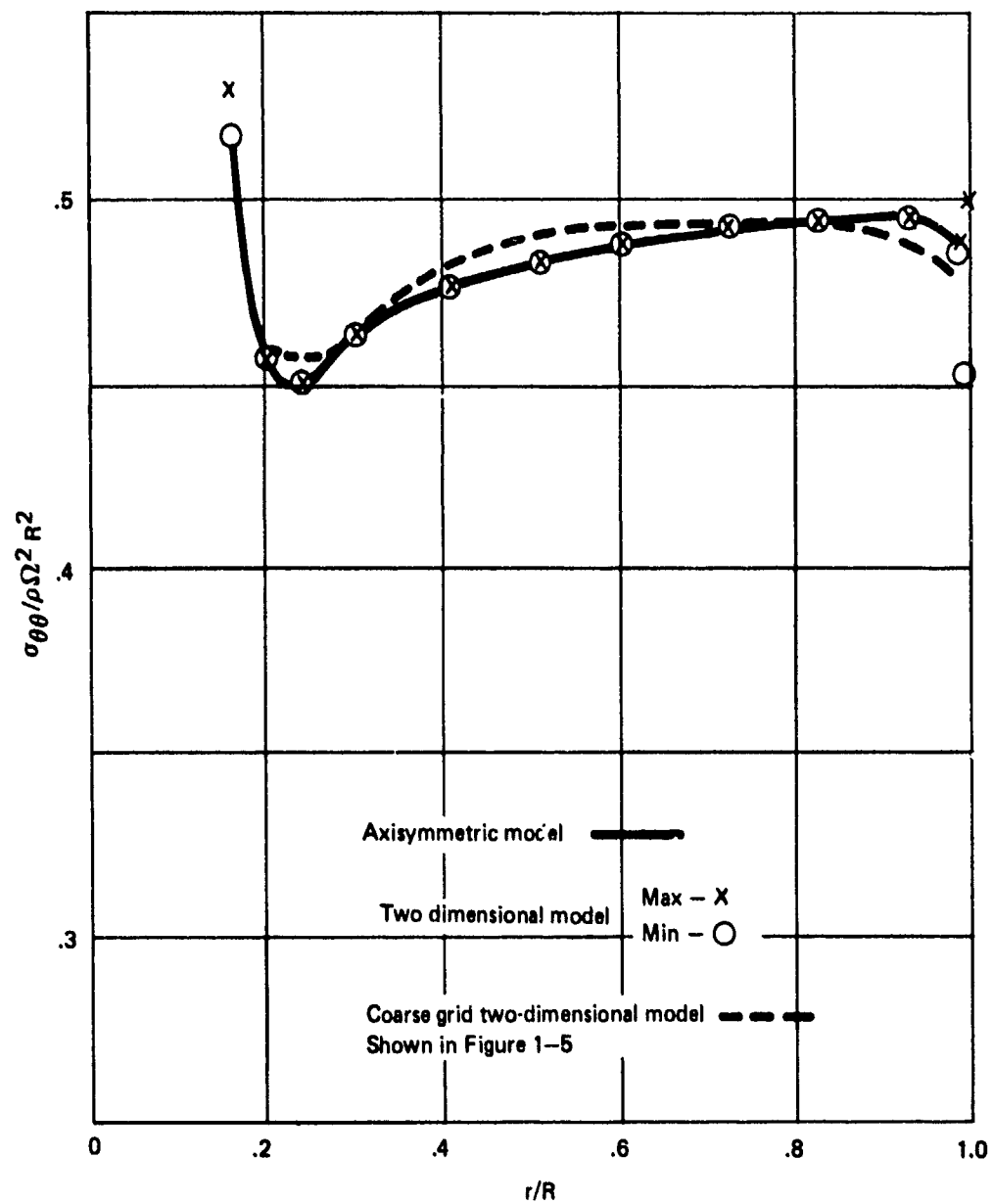
Figure 1—6. Original flywheel with degraded properties, comparison of hoop stresses in fiber direction $\sigma_{\theta\theta}$ in the hoop layer.

97-704
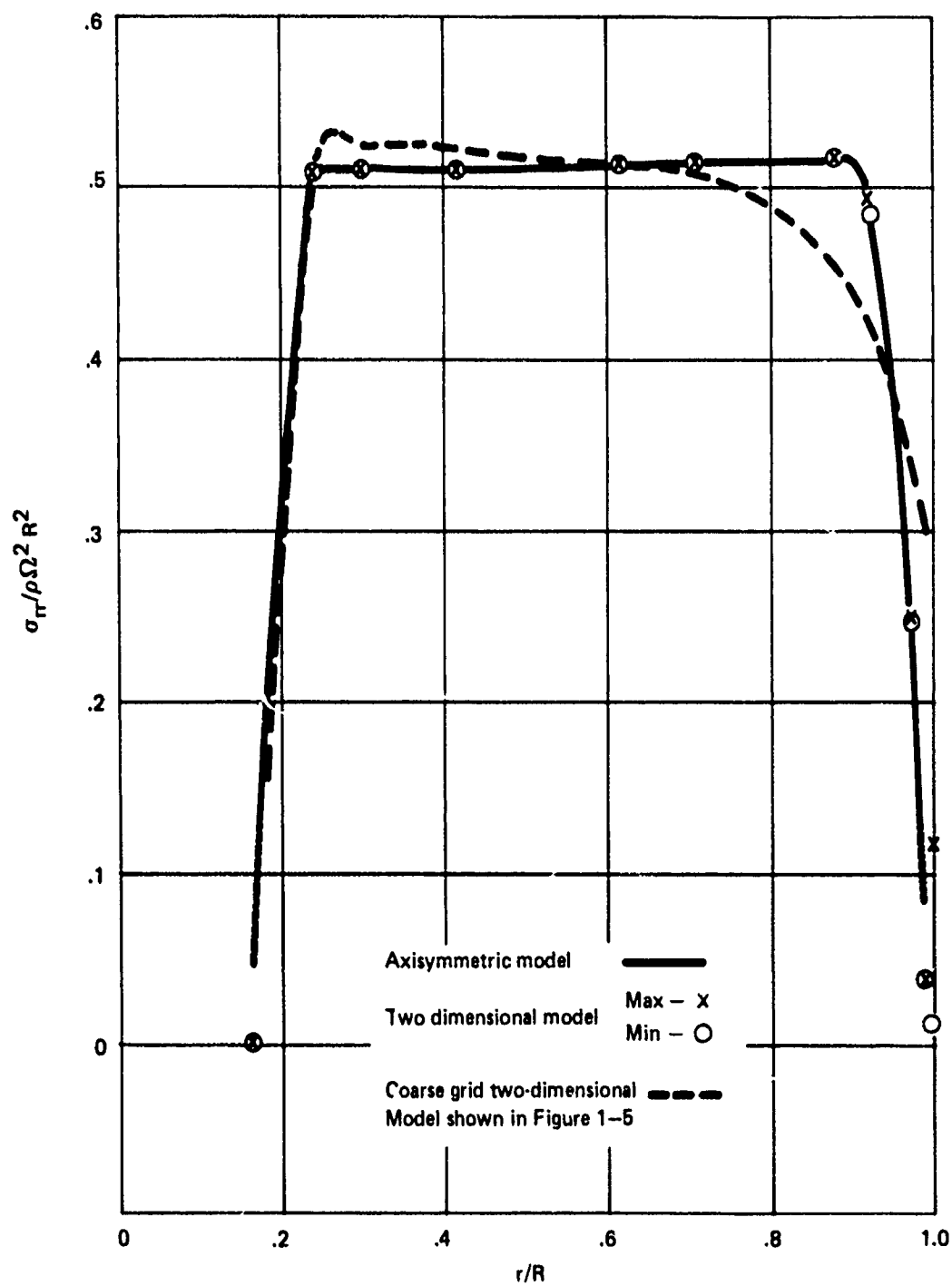
97-705

Figure 1—7. Original flywheel with degraded properties, comparison of radial stresses in the fiber direction σ_{rr} along the centerline of radial reinforcement.
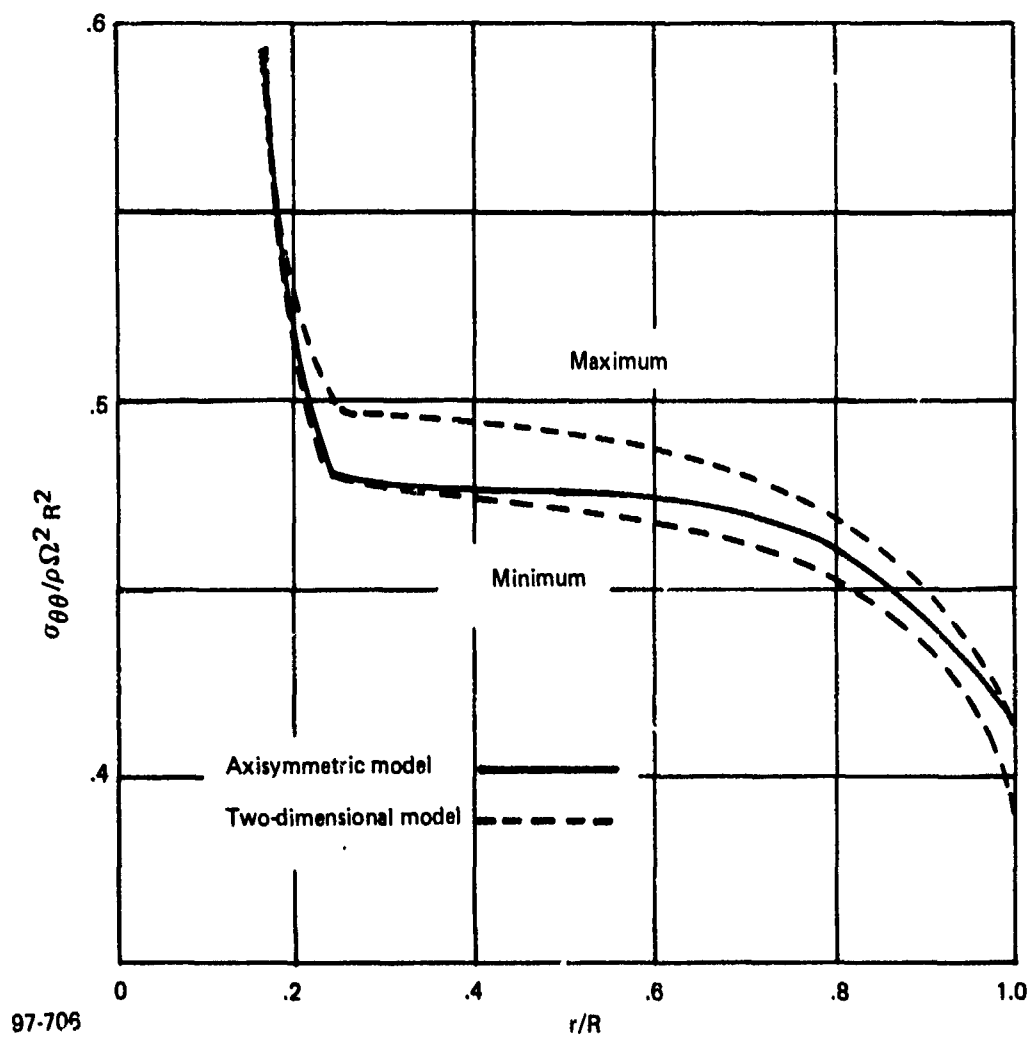
Figure 1–8. Original flywheel with undegraded properties, comparison of hoop stresses in the fiber direction $\sigma_{\theta\theta}$ in the hoop layer.

The 2-D finite element model indicates σ_{rr} approximately constant within radial with respect to θ.

*Center with respect to θ direction.

Axisymmetric model ——————

Two dimensional model — — — —

97-707
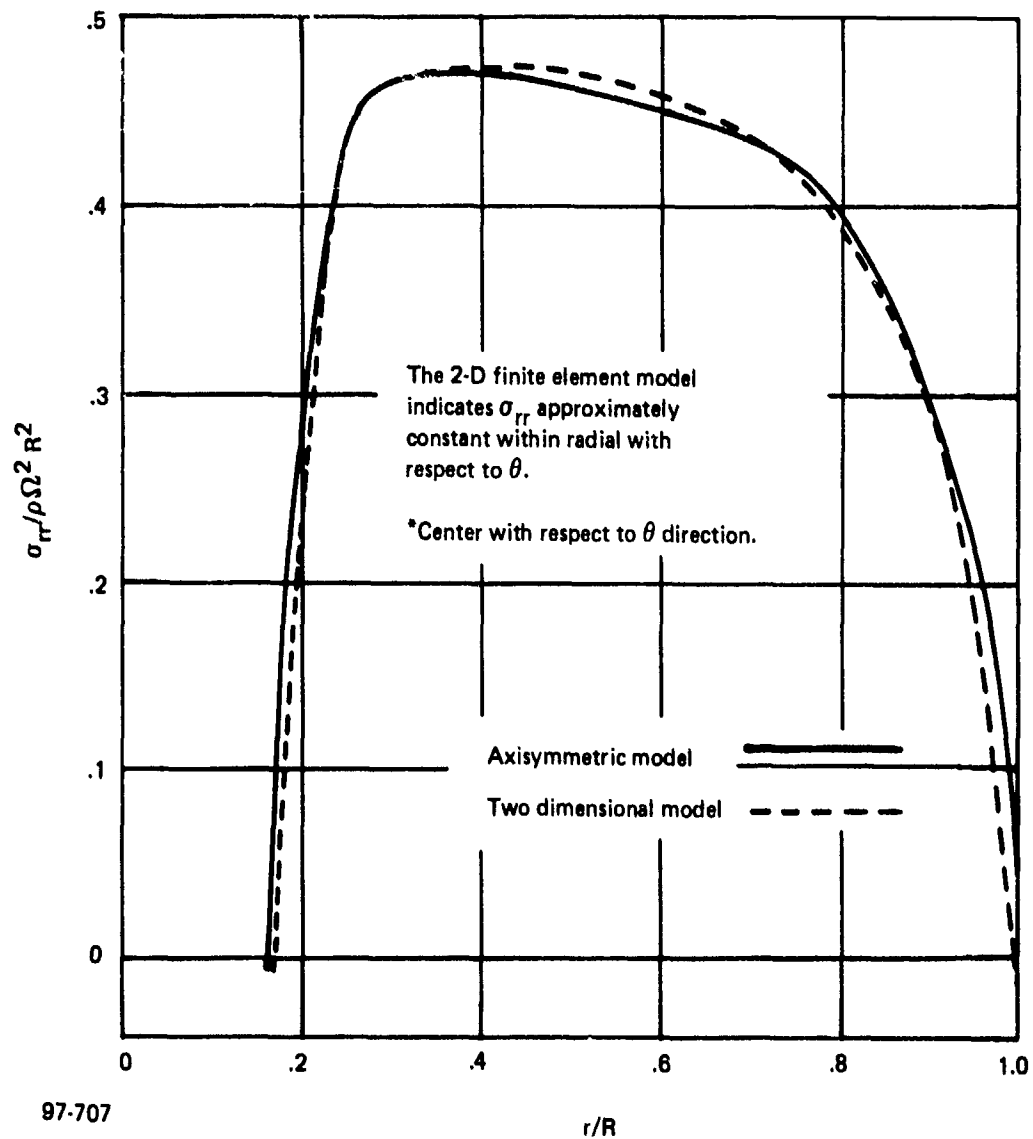
Figure 1—9. Original flywheel with undegraded properties, comparison of radial stresses in fiber direction σ_{rr} along centerline of radial reinforcement.*
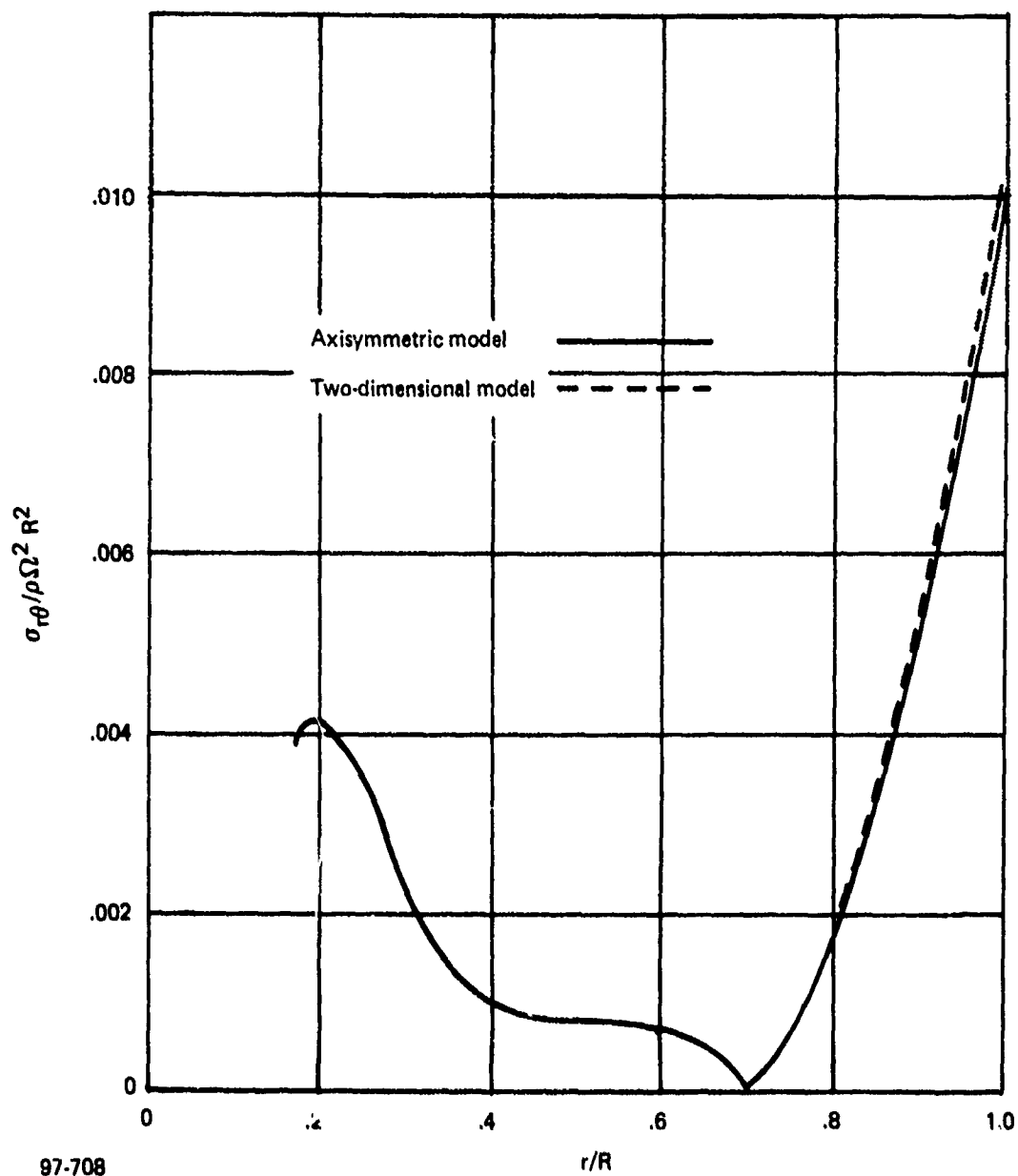
Figure 1—10. Original flywheel with degraded properties, comparison of shear stresses $\sigma_{r\theta}$.

97-708
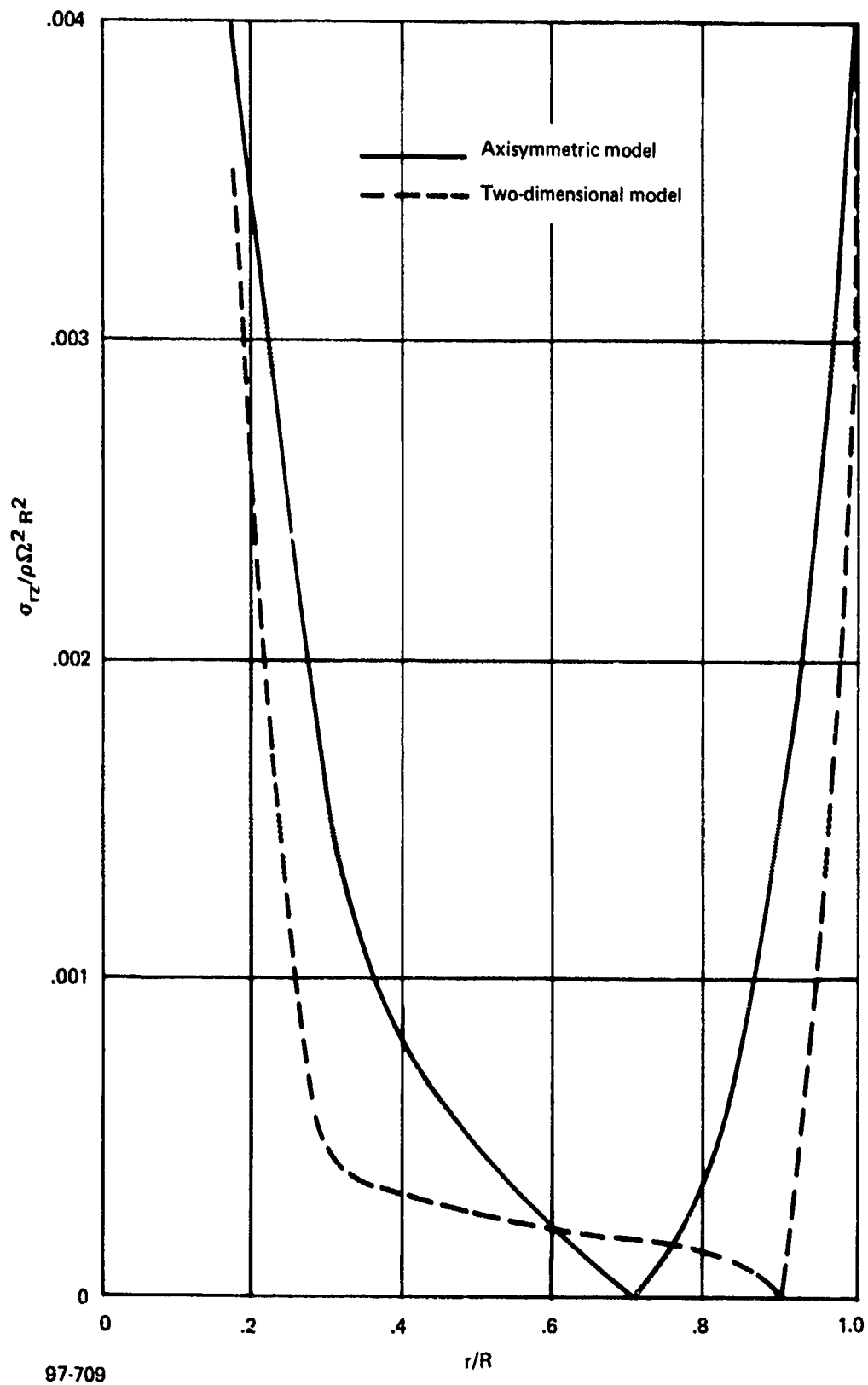
Figure 1–11. Original flywheel with degraded properties, comparison of shear stresses σ_{rz}.

97-709

present at the lateral free edge of a radial. It is believed that the differences shown in Figure 1-11 can only be resolved by a local 3-D finite element analysis in the region of the edge of the radial. Nevertheless, the maximum σ_{rz} stresses shown in Figure 1-11 differ only by 13 percent. Consequently, the differences between the models does not present a serious obstacle even for these σ_{rz} hoop-radial interlaminar shear stresses.

SECTION 2

ANALYTICAL ASSESSMENT OF EFFECT OF DEGRADED PROPERTIES

2.1 INTRODUCTION

In this section we investigate the effect of degraded material properties caused by the high biaxial stresses in the flywheel. The analytical results are obtained by using the two-dimensional finite element grid shown in Figure 1-4 and described in Section 1.

2.2 PRELIMINARY INVESTIGATION: UNDEGRADED VERSUS DEGRADED

As previously mentioned, the flywheel is designed using the $E_{90} = 0$, $\nu = 0$ degraded properties because of the low transverse (90°) strain allowable of Kevlar. The resulting flywheel has thus been optimized on the basis of the degraded properties. If the same configuration is analyzed using undegraded properties, the stress distributions are as shown in Figures 2-1 and 2-2. It is immediately apparent that the design was optimized for the degraded condition because the maximum stresses are substantially larger in the undegraded design, as summarized in the following table:

RESULTS FOR 2-D FINITE ELEMENT ANALYSIS

$\sigma_{r_{max}}$	Undegraded	Degraded
$\dfrac{\sigma_{r_{max}}}{\rho \Omega^2 R^2}$	.514	.605
$\dfrac{\sigma_{\theta_{max}}}{\rho \Omega^2 R^2}$	.530	.470
K_s (2-D Analysis)	.461	.404

This table also shows the shape factor K_s computed for these two cases and indicates a 12 percent lower K_s (and hence lower energy density) for the undegraded condition than for the degraded condition used to optimize the design.

2.3 EFFECT OF DEGRADED SHEAR MODULUS

A series of two-dimensional finite element runs were made to determine the effect of reducing the shear modulus G for the degraded properties shown in Section 1. The results shown in Table 2-1, are somewhat startling. They
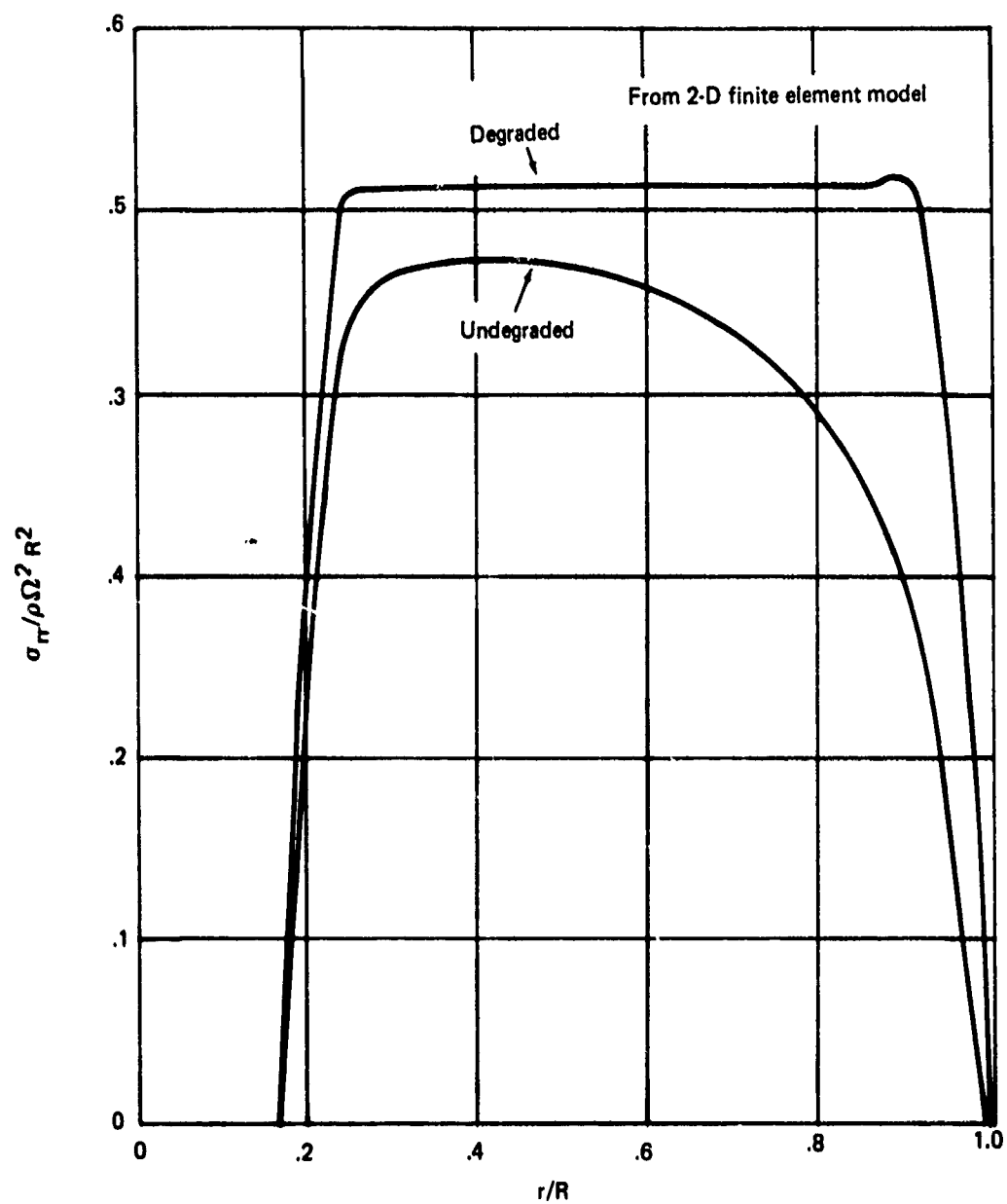
97-710

Figure 2—1. Degraded versus undegraded, comparison of radial stresses in fiber direction σ_{rr} along centerline of radial reinforcement.
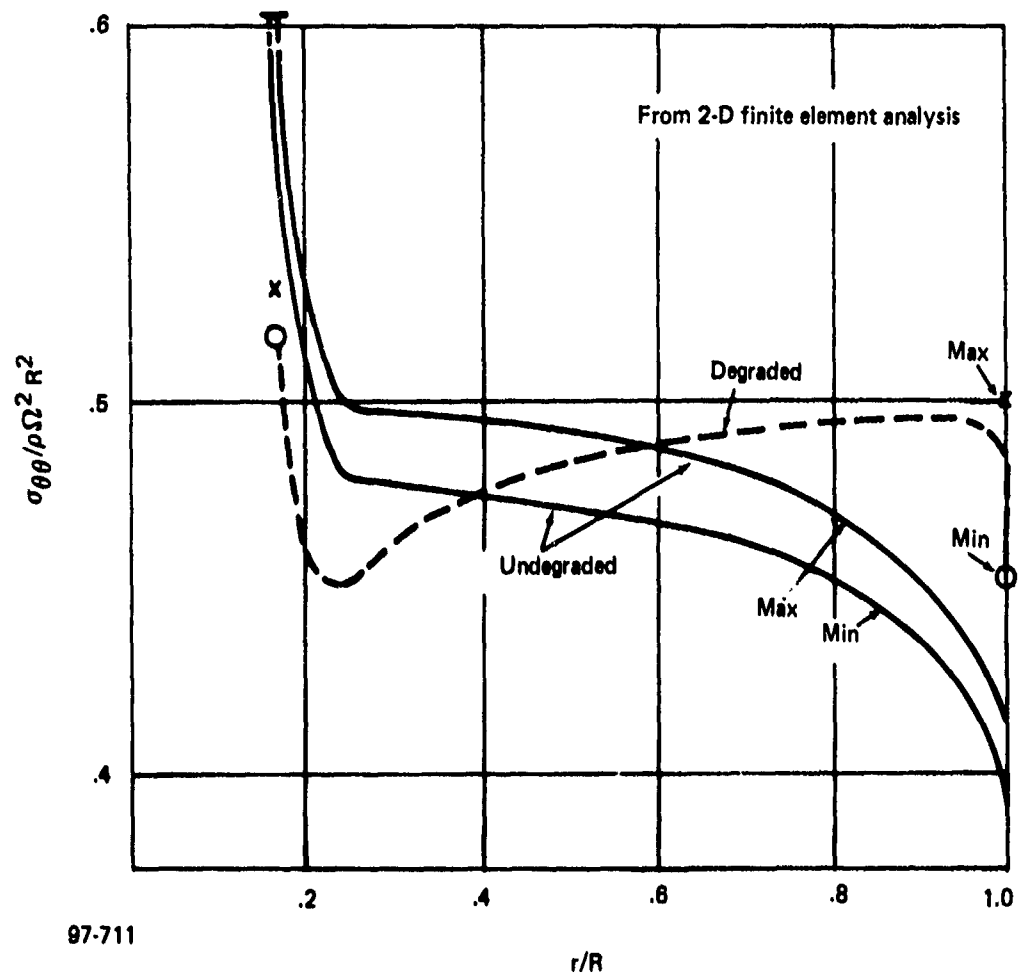
Figure 2—2. Degraded versus undegraded, comparison of hoop stresses in fiber direction $\sigma_{\theta\theta}$ in the hoop layer.

97-711

indicate that the maximum stresses and shape factor K_s are almost unaffected by reductions in the shear modulus down to one-tenth of the orginal. The distributions of the stresses shown in Table 2-1 are given in Figures 2-3 through 2-5 for the two cases $G/G_{orig} = 1$ and $G/G_{orig} = .1$. Although the figures show very little change in the maximum stresses with the reduction of G/G_{orig} to .1, they do indicate the beginnings of changes in the stress pattern. Figure 2-3 shows that as the shear modulus is lowered, the distribution of σ_r stresses in the circumferential direction across a radial becomes increasingly nonuniform. At $G/G_{orig} = .1$, as shown in Table 2-1, the nonuniformity is already sufficiently great for the radial stresses to become the maximum stresses in the wheel. Figure 2-4 shows a similar circumferential nonuniformity in the hoop stresses near the outside of the wheel as the shear modulus is reduced. These trends would indicate that the σ_r and σ_θ stresses will increase as G is reduced below .1.

TABLE 2-1. EFFECT OF DEGRADED SHEAR MODULUS
(FROM 2-D FINITE ELEMENT ANALYSIS)

$G/G_{original}$	1.0	.5	.1
$\dfrac{\sigma_{r_{max}}}{\rho \Omega^2 R^2}$	.514	.517	.526
$\dfrac{\sigma_{\theta_{max}}}{\rho \Omega^2 R^2}$	.530	.529	.523
$\dfrac{\sigma_{rz}}{\rho \Omega^2 R^2}$	.00355	.00356	.00354
$\dfrac{\sigma_{r\theta}}{\rho \Omega^2 R^2}$	.01032	.00958	.00947
K_s	.461	.462	.465

Implications of this result are as follows. First, within the range of G degradations considered it indicates that the dominant effect on flywheel efficiency will come from reduced shear stress allowables rather than from the reduced modulus. The differing effects of shear modulus and shear allowables are illustrated, by example, in Section 2.4. Second, the results indicate that G/G_{orig} must be reduced below .1 to alter the stresses σ_r and σ_θ sufficiently to effect the overall flywheel shape factor K_s. Further evaluation of extremely degraded G cases is being continued at the present time.

-30-
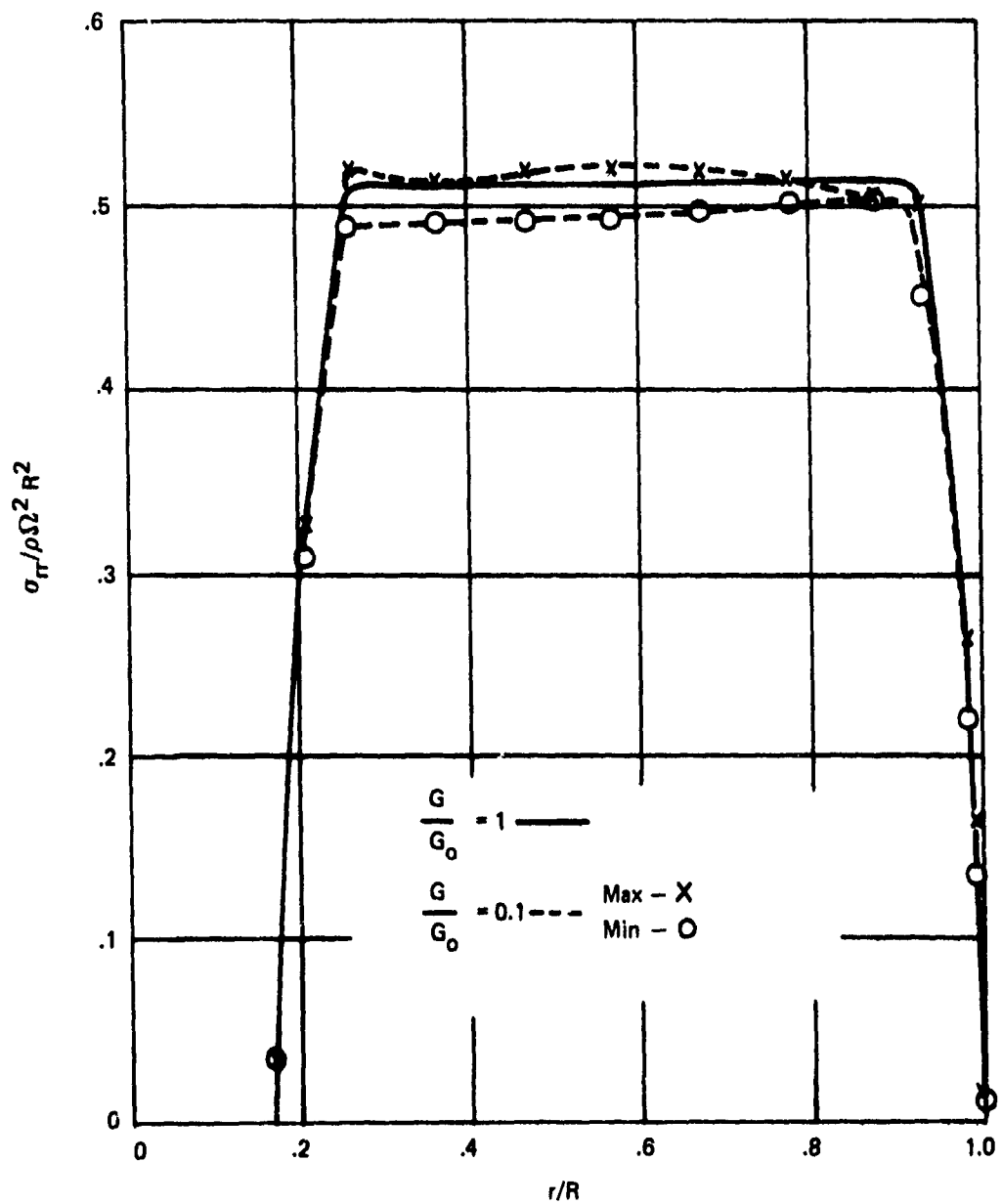
97-712

Figure 2–3. Comparison of radial stress distribution for undegraded and degraded shear moduli.
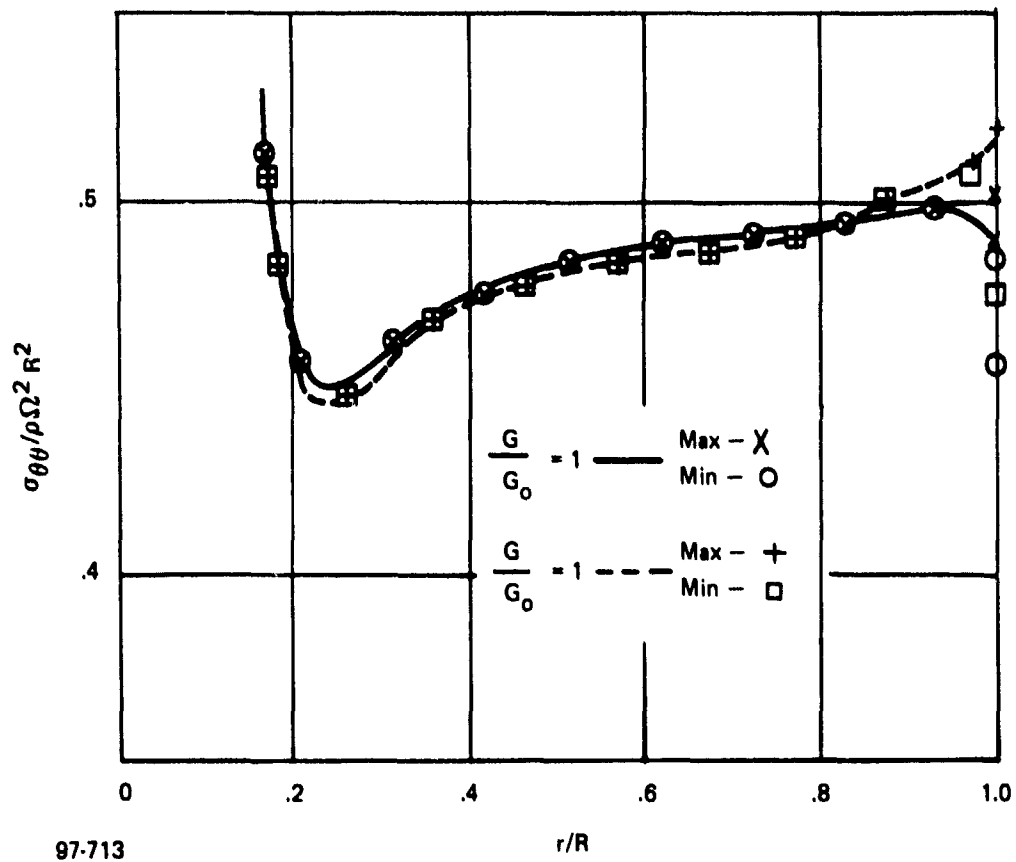
Figure 2–4. Comparison of hoop stress distribution for undegraded and degraded shear moduli.
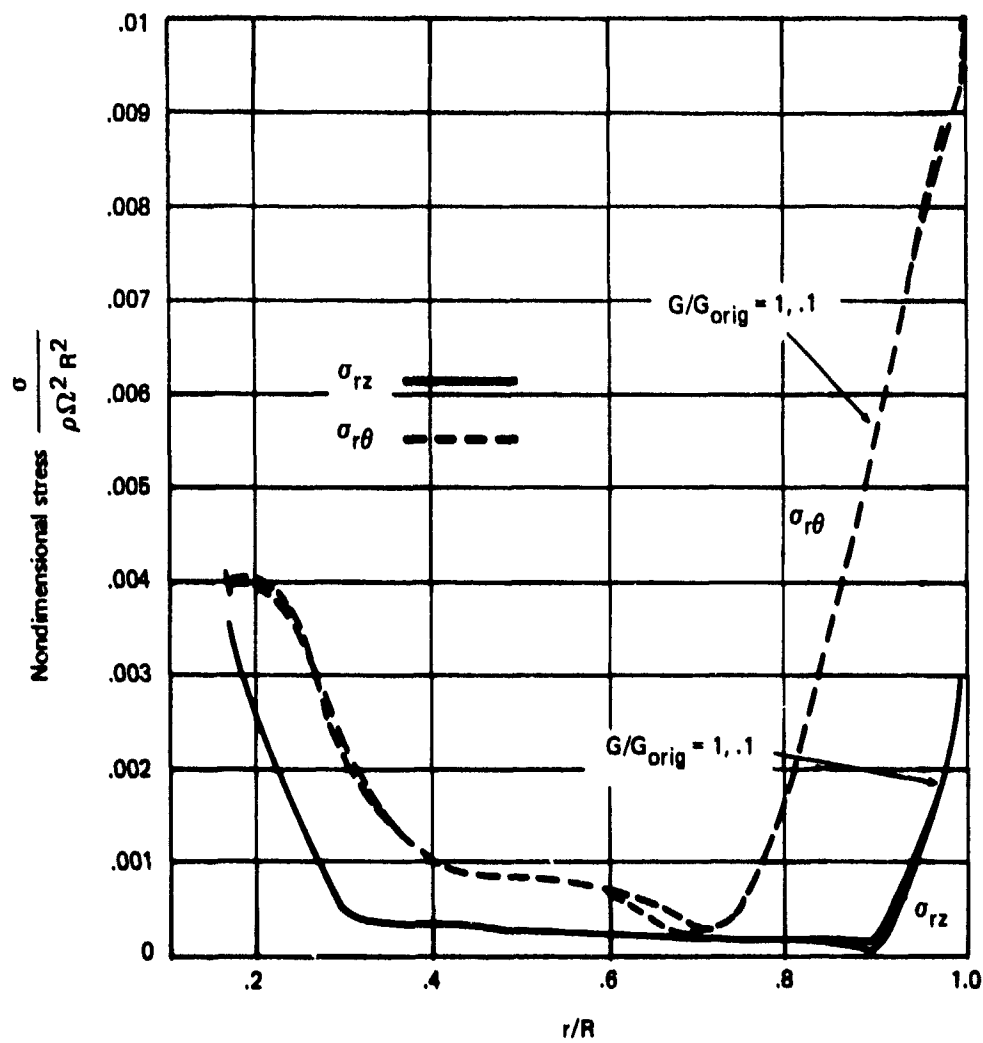
Figure 2—5. Effect of reduction in shear moduli on shear stresses σ_{rz} and $\sigma_{r\theta}$.

97-714

2.4 CORRELATION OF PREDICTIONS WITH MEASURED DEGRADATION

We now correlate the analytical predictions with the property degradation measured experimentally and reported in Section 5. The experimentally determined shear modulus ratio $G/G_{original}$ is .825 and falls within the range covered by Table 2-1. This indicates that the wheel stresses are essentially unaffected. The reduction in shear strength to .728 of the undegraded strength, however, indicates lower margins of safety with respect to shear failure for the degraded case. For the undegraded case the margin of safety on the $\sigma_{r\theta}$ stress, computed from the values shown in Table 1-1, is (7.9/3.9)-1 = 1.02. For the experimentally measured degraded shear strength it is (5.75/3.9)-1 = .47, so that the margin is reduced roughly by half but nevertheless remains positive.

The greater sensitivity of the margins to shear strength rather than shear modulus can be further illustrated by considering two hypothetical cases and the resulting margins of safety as follows:

| | Percent of undegraded values | | |
Case	For G	For σ_{12} allowable	Margin of safety
Case 1	100%	40%	-.19
Case 2	40%	100%	+1.0
Undegraded Case	100%	100%	+1.0

The table indicates greater sensitivity of margins to the σ_{12} shear allowable. However, it should be pointed out that this computation of margins based on $\sigma_{r\theta}$ and the shear allowable may be conservative because even if the σ_{12} shear strength is lost, the performance of the wheel may not be degraded due to catenary-like action of the degraded hoop reinforcements.

Because the experimental results apply to the case of 52 percent of the ultimate $0°$ stress, it is possible that the degradation of in-plane shear strength may limit the flywheel performance at higher percentages of the ultimate load. Such a problem, if it occurs, could be ameliorated by increasing the number of radials and thereby reducing the $\sigma_{r\theta}$ stresses.

SECTION 3

SENSITIVITY STUDIES

3.1 INTRODUCTION

Sensitivity studies were carried out to evaluate the effect of property variations and geometric variations associated with manufacturing and fabrication. The studies included in Subsections 3.2 and 3.3 involve axisymmetric variations and use the axisymmetric finite element code. In Section 3.4 asymmetric effects are investigated by use of the two-dimensional finite element model shown in Figure 1-5. In this latter investigation the effect of asymmetric variations on the imbalance of the flywheel are considered.

3.2 VARIATIONS IN FIBER VOLUME

Here we consider the effect on the flywheel stresses and efficiency of axisymmetric variations in the fiber volume ratio V_f. Two specific cases are considered: (1) the case of one constant value of V_f for the radial layers and another constant value for the hoop layers, and (2) a case of a local variation of V_f within the hoop layer alone.

For both of these cases we assume the following properties for the Kevlar 49 fiber and epoxy matrix:

Modulus of fiber $= E_f = 20 \times 10^6$ psi
Modulus of matrix $= E_m = .5 \times 10^6$ psi
Fiber weight/volume $= \rho_f g = .053$ lb/in^3
Matrix weight/volume $= \rho_m g = .0426$ lb/in^3

The Kevlar 49 properties are those given by duPont.* Typical matrix properties are used.**

The mechanical properties for a composite are formulated by using the rule of mixtures, namely:

$$E_1 = E_f V_f + E_m (1-V_f)$$

$$\rho_g = \rho_f g V_f + \rho_m g (1-V_f)$$

The resulting values of E as a function of V_f are given in Figure 3-1. It should be pointed out that for $V_f = .59$ one has the reference properties $E_1 = 12 \times 10^6$ psi and $\rho g = .0487$. These correspond to the properties cited in Section 1.

Case 1: Different V_f's for Hoops and Radials

In this case we fix $V_f = .59$ for the radial reinforcements and vary V_f for the hoop reinforcements over the range $V_f = .45$ to $V_f = .70$. Thus we

---

*Hunter, R. L., "Characteristics and Uses of Kevlar 49 High Modulus Organic Fiber," duPont Report, revised 9/18/73.
**Ashton, J. E., Halpin, J. C., and Petit, P. H., "Primer on Composite Materials: Analysis" Technomic Publishers, 1969.
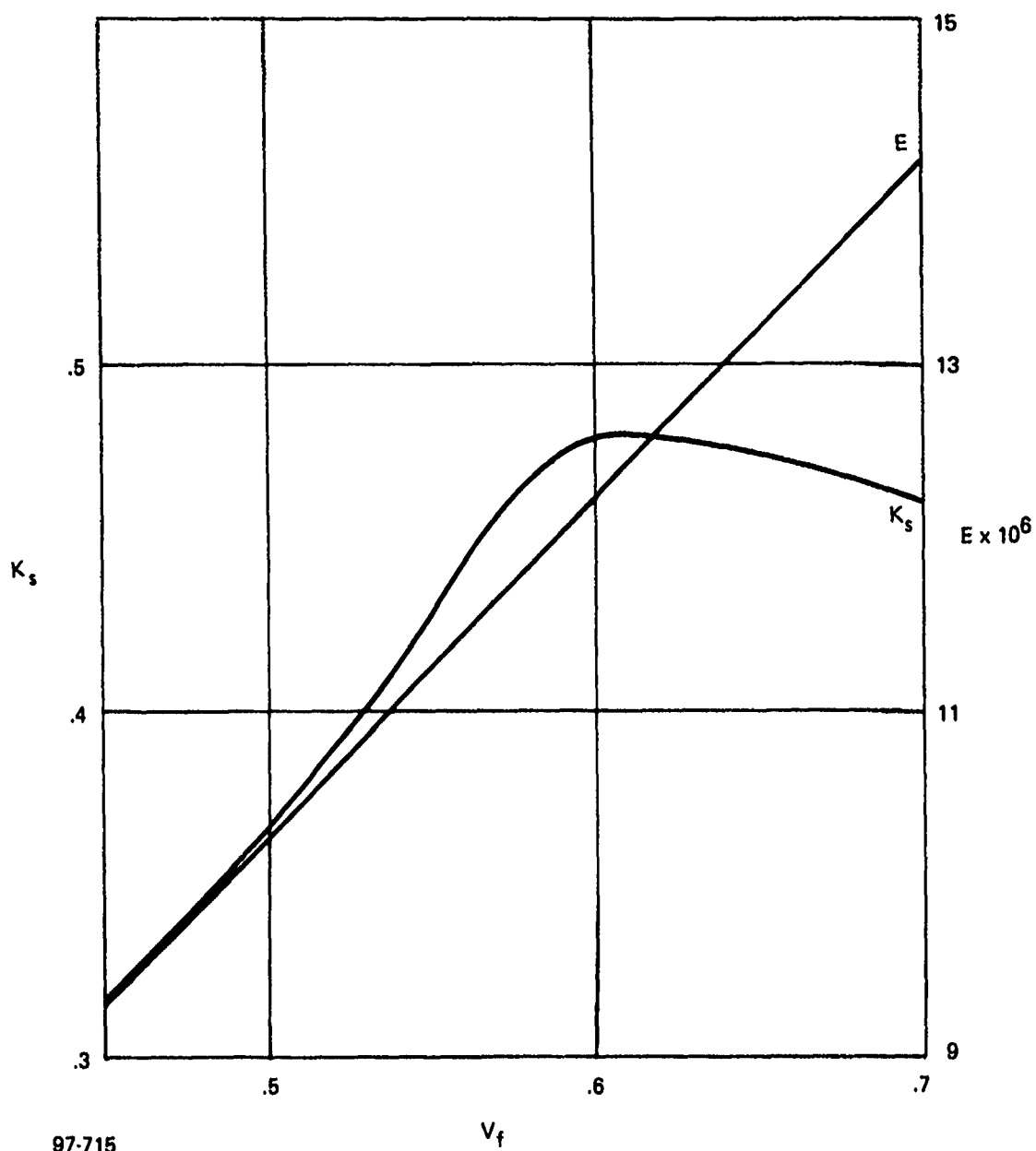
Figure 3–1. Variation of modulus and shape factor K_s with volume fraction V_f.

97-715

are assigning the radials the reference properties and we are varying the properties of the hoops. Results were obtained by parametrically running the axisymmetric finite element wheel code. Stress distributions obtained in this case are shown in Figure 3-2.

In order to determine the effect of V_f on the wheel efficiency it is necessary to postulate the dependence of the strength on V_f. This was determined on the basis of an allowable strain criterion. Consequently the 0° strength is assumed to be proportional to the modulus, which is shown in Figure 3-1.

In order to express these parametric results in terms of energy density or a shape factor K_s a problem in definitions arises. If we solve the equation in Section 1.2 for K_s we get:

$$K_s = \frac{\text{Kinetic Energy}}{\text{Weight}} \cdot \frac{\rho g}{\sigma}$$

The problem is to decide what values of ρg and σ to use for Case 1 in which two different sets of properties occur. The choice used in this work is to take ρg and σ as the reference values, i.e., those for $V_f = .59$. Having done this, all variations of kinetic energy per unit weight with V_f are reflected in corresponding variations of K_s. The results calculated on this basis are shown in Figure 3-1 which shows K_s decreasing as one moves away from $V_f = .59$, the volume fraction for which the wheel design is optimized. As might be expected, the figure shows that K_s drops more rapidly as V_f is decreased. The results shown in Figure 3-3 for $\sigma_{r\theta}$ and σ_{rz} as functions of V_f do not indicate very great variations within the range $V_f = .45$ to $.70$, and are not expected to significantly limit the design.

Case 2: Local Variations of V_f in Hoops

In this case we consider the effect of a local axisymmetric variation in the hoop layer. The postulated variation of V_f is shown in Figures 3-4 and 3-5 together with the stress from the axisymmetric analysis. Also shown in these plots are the relative changes in strength postulated on the basis of strain to failure. The resulting shape factor K_s is .447, 9 percent down from .474 of the original design.

3.3 VARIATIONS IN HOOP AND RADIAL GEOMETRIES

Three different types of variations in the geometry of the hoop and radial reinforcements were studied:

1. Variations of hoop thicknesses,

2. A .010 inch change in radial width,

3. A +.010 inch, -.010 inch combination change in radial width.
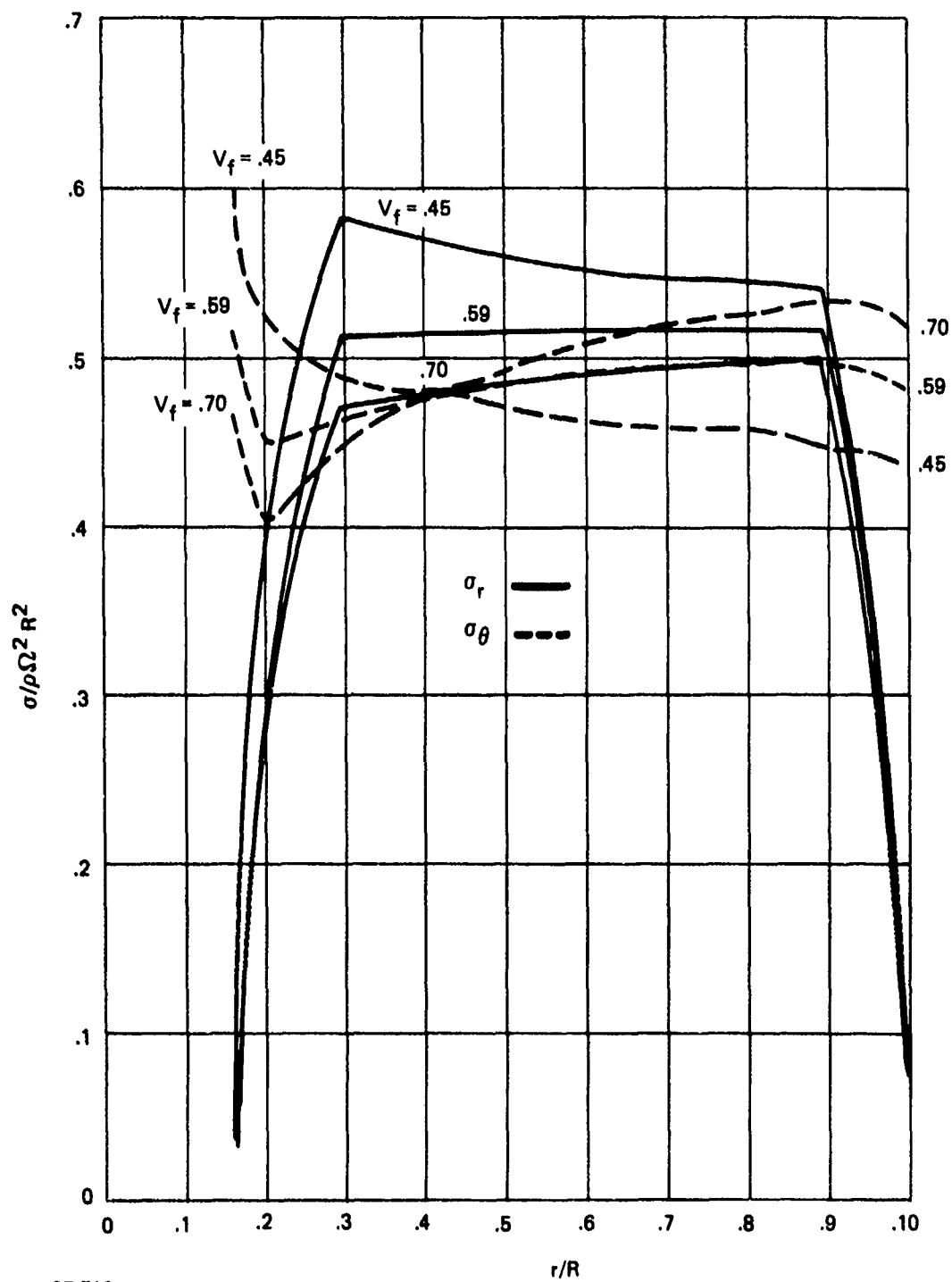
Figure 3—2. Stress distributions versus hoop fiber volume ratio.

97-716

-38-
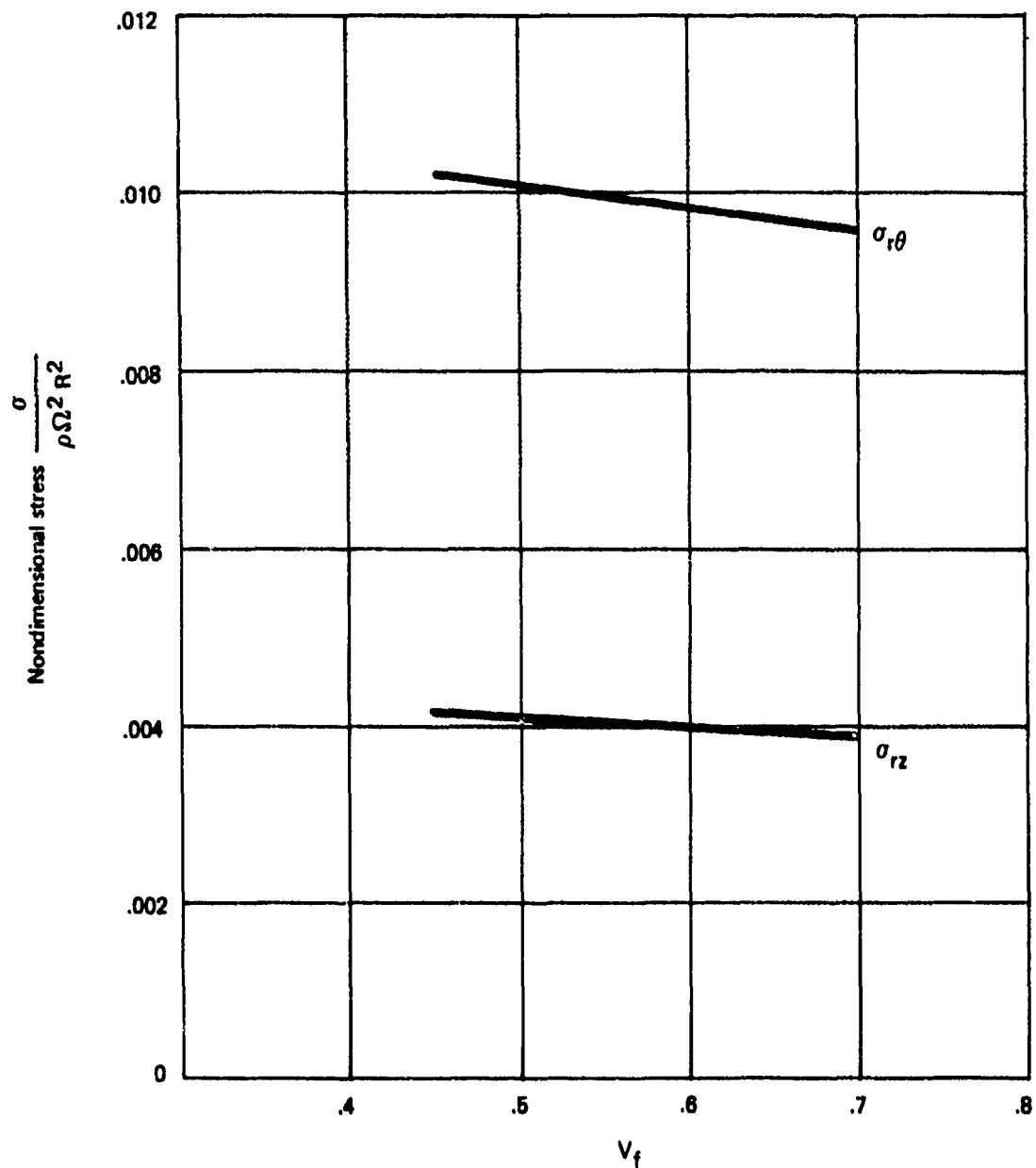
Figure 3–3. Variations of σ_{rz} and $\sigma_{r\theta}$ with fiber volume ratio V_f, for V_f = .59 for radials, V_f varies for hoop.

97-717

-39-
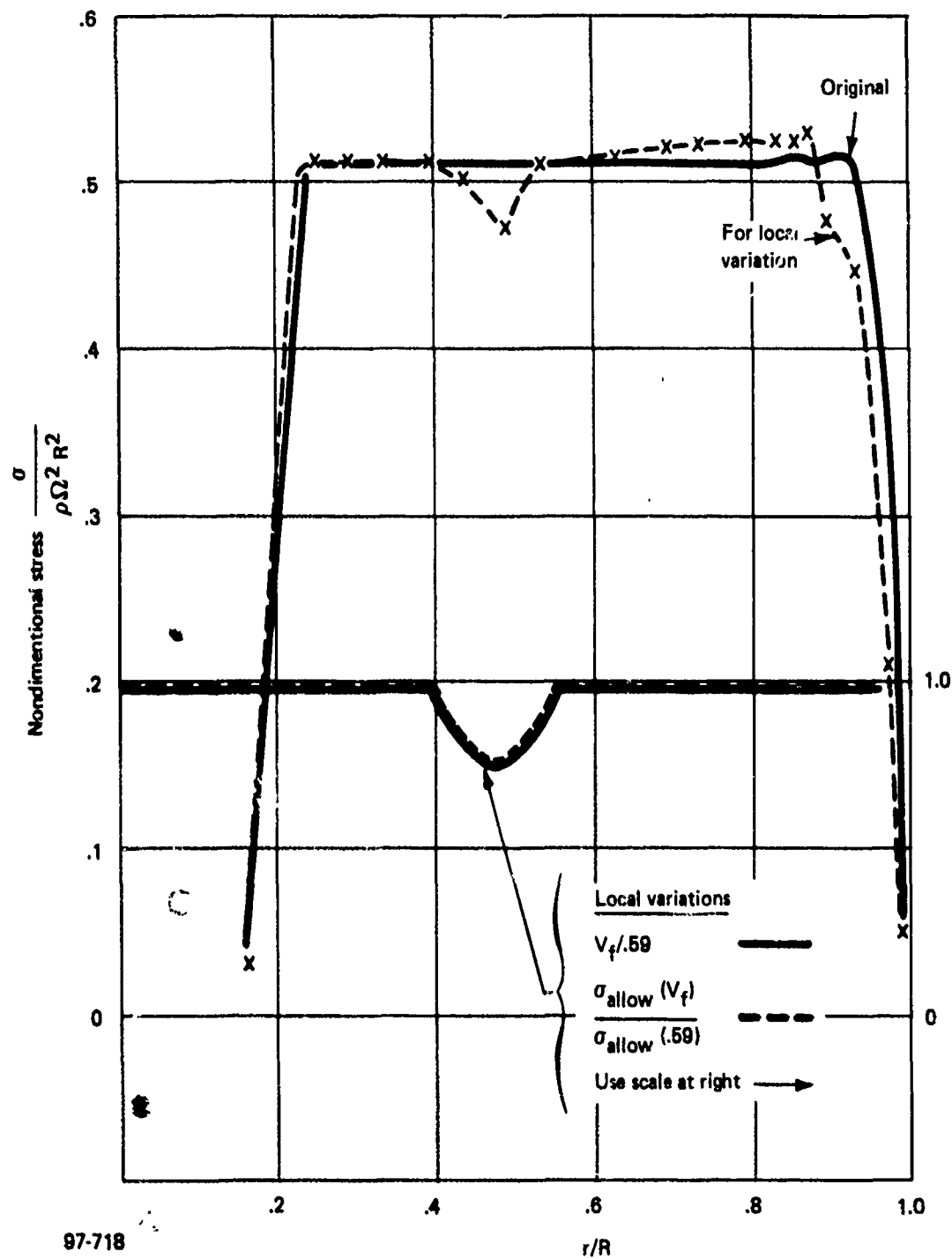
Figure 3—4. Radial stress distribution for local variation of V_f in hoop layer.

97-718
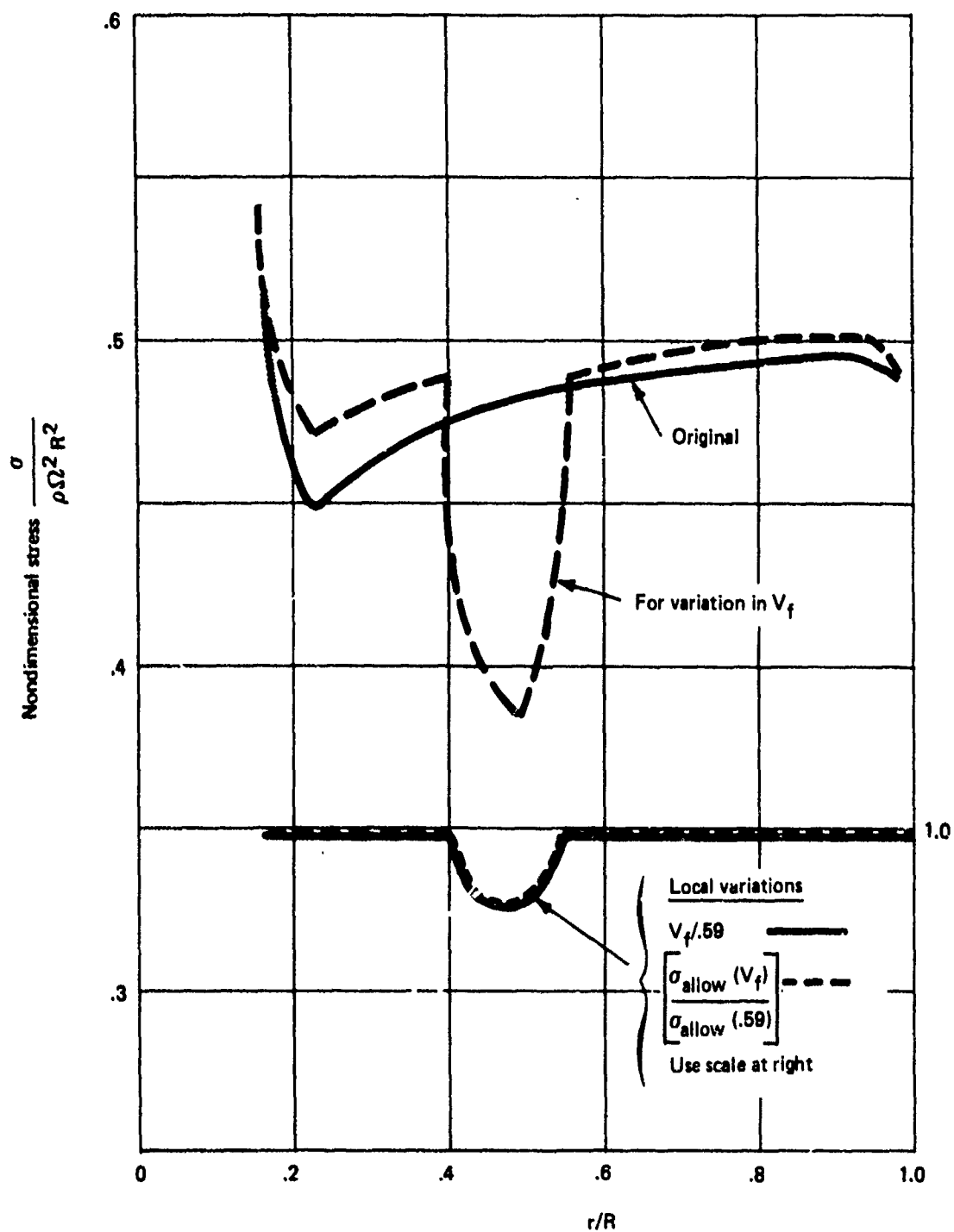
Figure 3—5. Hoop stress distribution for local variation of V_f in hoop layer.

97-719

-41-

Variations of Hoop Thickness

Results obtained by varying the hoop thickness are shown in Figures 3-6 through 3-8. Figure 3-6 shows the changes in stress distribution that occur as the hoop thicknesses are perturbated away from the design configuration. The figure indicates that as the hoops are thickened (+20%) the radials become overstressed and the hoops understressed. When the hoop thickness is reduced (-20%) the reverse occurs: the hoops are overstressed and the radials become understressed. These results clearly show the optimal feature of the unperturbed (0%) original design thickness combination. The corresponding changes in shape factor K_S are shown in Figure 3-7. A 20 percent reduction in hoop thickness results in a 19 percent decrease in K_S; a 20 percent increase in hoop thickness lowers K_S by only 10 percent. The wheel appears to be more sensitive to decreases in hoop thickness because of the tendency for high hoop stresses to occur at the inside edge of the wheel.

It should be pointed out that these calculations apply equally well to changes in radial thickness, that is, the results are dependent on the ratio of hoop to radial thickness.

In Figure 3-8, the corresponding σ_{rz} hoop to radial interlaminar shear stresses are plotted. The special nondimensional form of stress shown in the figure relates the shear stress to the maximum stress so that the significance of the shear stress changes can be evaluated. We presume that the wheel will be spun up to a speed Ω for which the maximum σ_r or σ_θ stresses reach the material allowable -- consequently the ratio σ_{rz}/σ_{max} is a key parameter and is used in representing the results in Figures 3-8 and 3-11. The ordinates of these figures are expressed in terms of a shear stress parameter $(\sigma_{rz} \cdot R)/\sigma_{max} \cdot h_r)$. Figure 3-8 shows that the effect of changing hoop thicknesses of ±20% does not substantially influence the σ_{rz} shear stress parameter.

.010-inch Change in Radial Width

In the reference design the radial reinforcements are .048 inch wide on the inside (r = 1.625"), .191 inch wide at r = 4.85 inch and .045 inch wide at the outside r = R = 9.75 inch. We now consider two cases one with .010 inch added to the radial width, and one with .010 inch subtracted from the radial width. The resulting stress distributions and resulting change in shape factors are shown in Figures 3-9 and 3-10. The distributions are very similar and there is a small change in K_S of approximately 8 percent for the +.010 and -.010 changes in radial width. The dominant effect, however, is a change in maximum σ_{rz} interlaminar shear stresses because from a percentage point of view the .010 inch change has the greatest effect near the inside and outside edges of the wheel where the shear stresses are greatest. The changes in shear stress parameters are shown in Figure 3-11, which shows an increase of 14 percent for the radial which is .010 inch narrower.

+.010 inch, +.010 inch Combined Change in Radial Width

A combined case was run in which the width of the outer half (larger r) of the radial was reduced by .010 inch and correspondingly increased on the
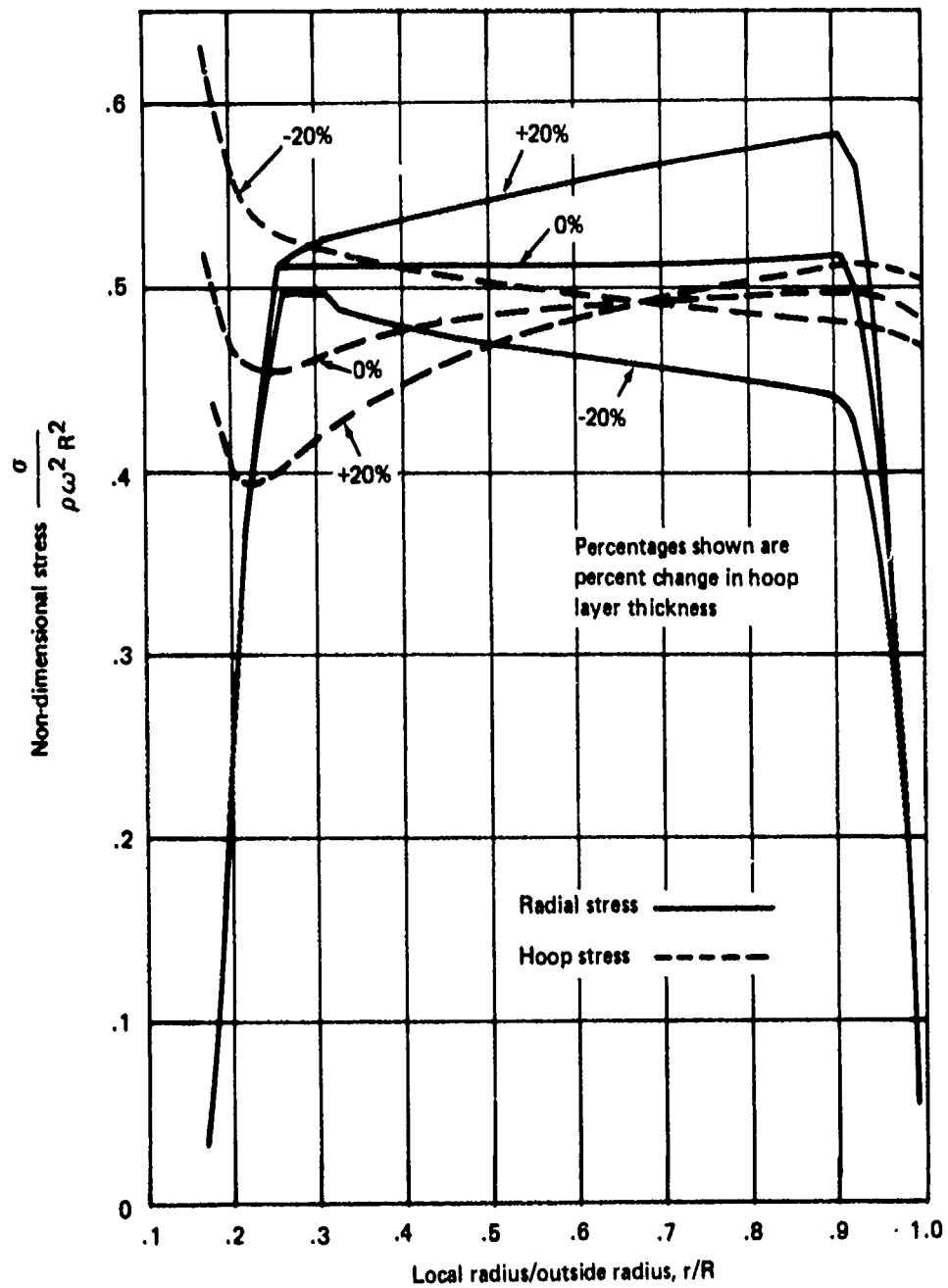
Figure 3—6. Sensitivity of stresses to hoop layer thickness.

97-720

-43-
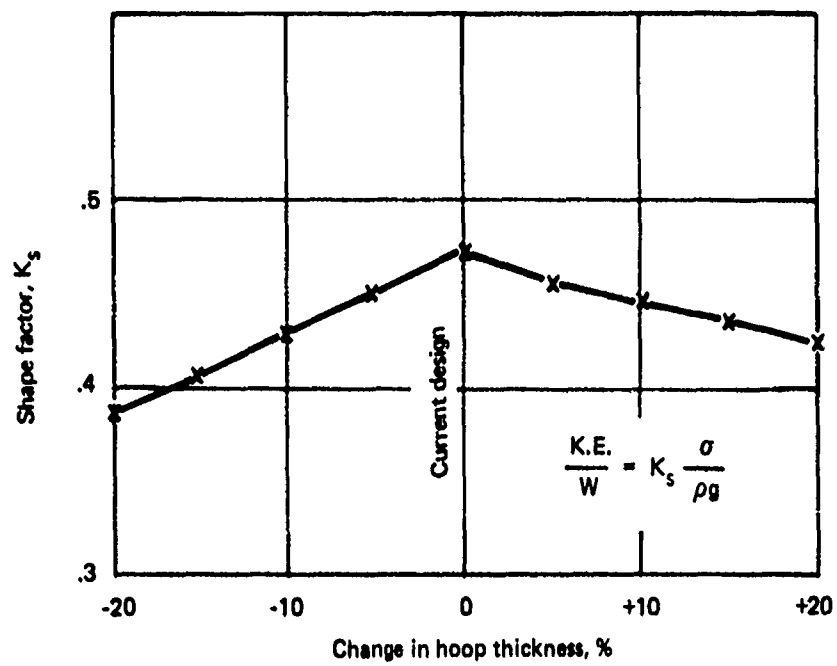
Figure 3—7. Sensitivity of shape factor to hoop layer thickness.

97-721
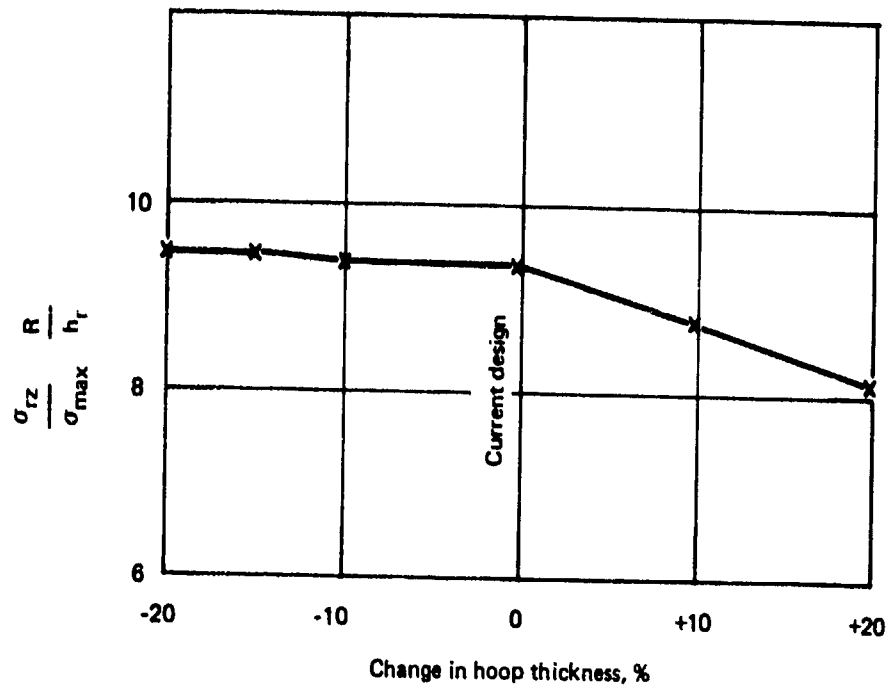
97-722

Figure 3—8. Sensitivity of shear stresses to hoop layer thickness.
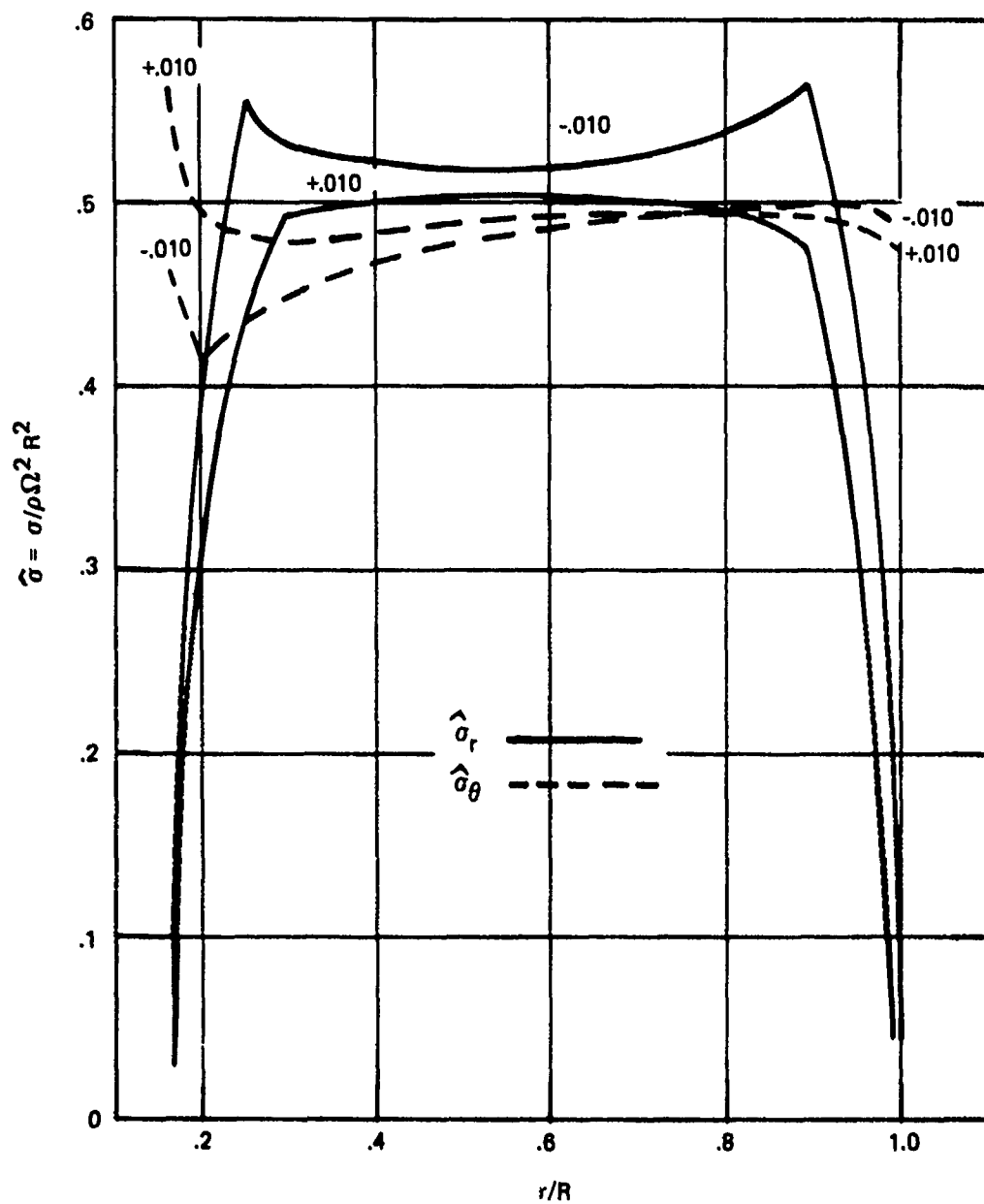
97-723

Figure 3–9. Stress distributions versus radial width variations for +.010 and -.010 inch changes in radial width.
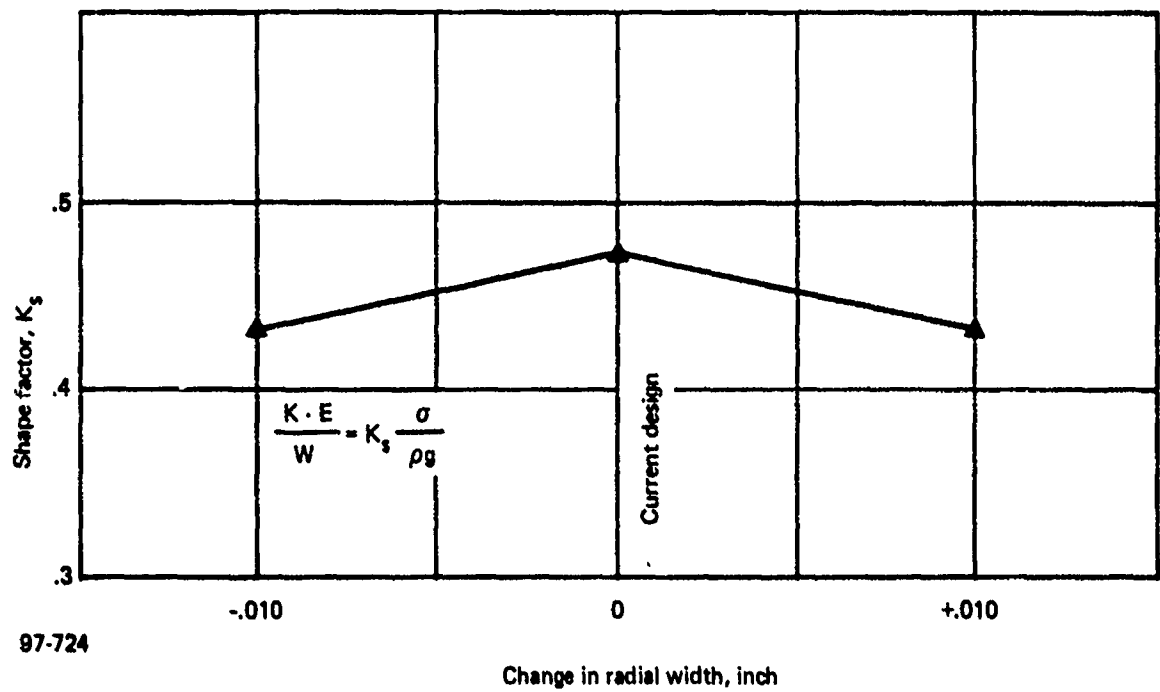
Figure 3—10. Sensitivity of shape factor to radial width.

$$\frac{K \cdot E}{W} = K_s \frac{\sigma}{\rho g}$$

97-724

-47-
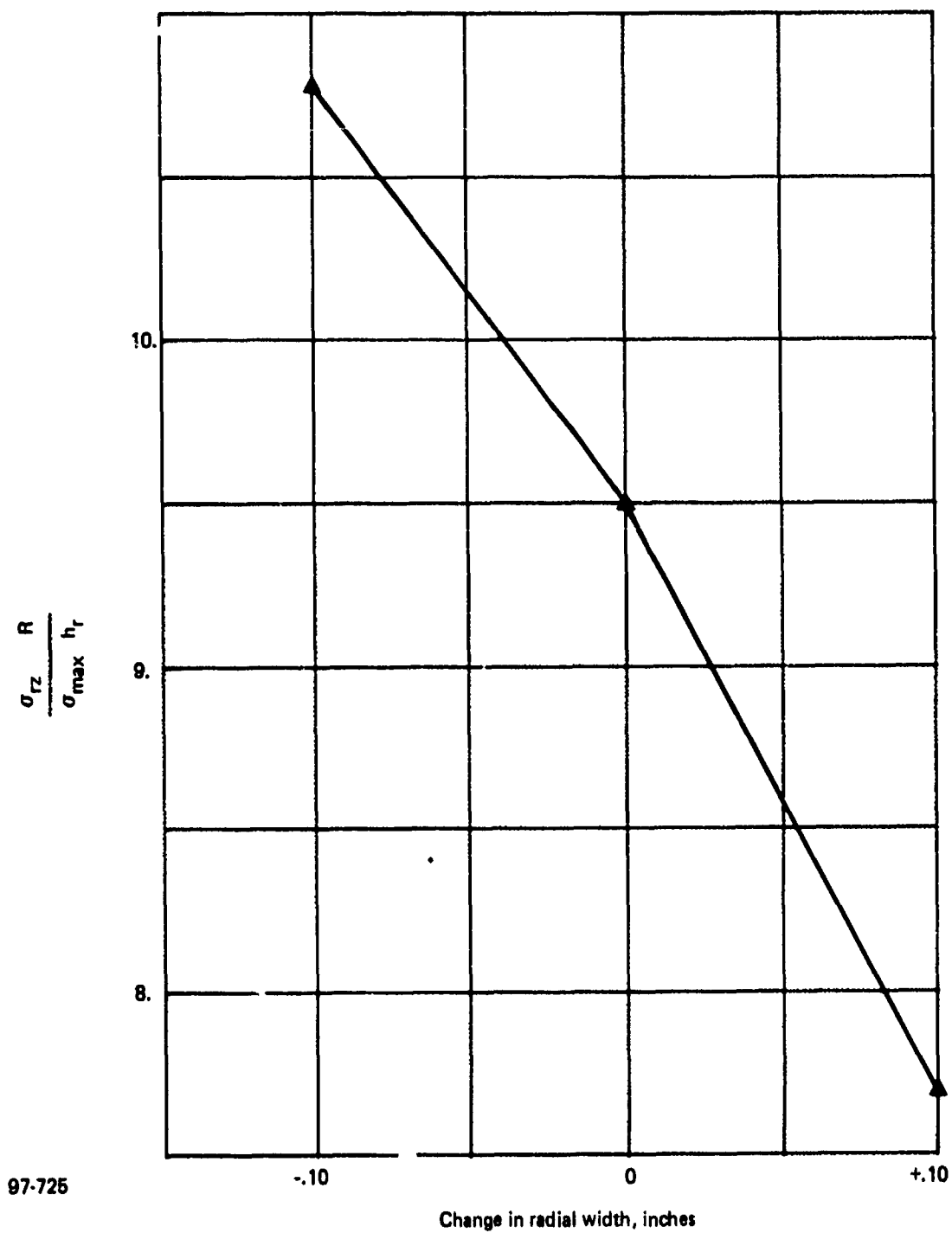
Figure 3—11. Sensitivity of shear stress σ_{rz} to radial width.

inside half (smaller r). The result was K_s = .429, a 9 percent reduction from the design case. The shear stress parameter $(\sigma_{rz} \cdot R)/(\sigma_{max} \cdot h_r)$ is 14 percent higher in this case.

It should be pointed out that, for the +.010 inch, -.010 inch and combined ±.010 inch cases, that the maximum $\sigma_{r\theta}$ shears are not greatly affected.

3.4 EVALUATION OF ASYMMETRIC PROPERTY VARIATIONS

Asymmetric property variations were evaluated using the finite element grid shown in Figure 1-5. The model "smears out" the radials in the circumferential direction. Two cases of asymmetric variations of the modulus, as shown in Figure 3-12, were analyzed. In Case A the modulus of the radials is varied; in Case B the modulus of the hoops. The change in stresses for these cases is as follows:

Case	Change in modulus	Change in maximum stress
A	±5%	+3.9%
B	±1%	+.1%

A major reason for carrying out these asymmetric property variation studies is to compute the imbalance due to deformation of the wheel. To do this we evaluate the shift in centroid of the wheel (relative to Point A of Figure 3-12) that would exist when σ_{max} = 200 ksi. A typical wheel weight of 16.86 pounds was used in the calculations. The results presented in tabular form appear below:

Case	Change in modulus	Distance of centroid shift (inch)	Imbalance for 16.86 pound wheel (inch-grams)
A	±5%	.00416	36.19
B	±1%	.000504	6.9

The resulting imbalances shown above are considerably in excess of the imbalances that remain after balancing the wheel which are of the order of 1 inch-gram. It should be recognized that the ±5% and ±1% variations used in the study are highly unlikely to occur because they represent averages of all the deviations in modulus through the thickness as well as in the in-plane directions. The variations used in this study are conservative estimates of asymmetries in an individual layer. Random layer orientation during assembly and inter-layer load sharing during operation will tend to distribute displacement more evenly. The method of fabricating the hoops is more likely to generate axisymmetric rather than asymmetric variations in modulus. Similarly, the radials are stamped out of sheets of Kevlar tape and are expected to be very regular.

Case A

$E_\theta = E$

$R_r = 1.05E$

A

$E_r = .95E$

KEY
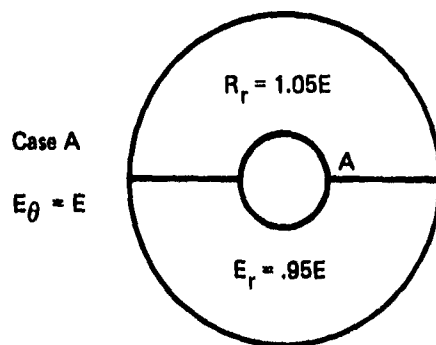
E_θ = Modulus of hoops

E_r = Modulus of radials

E = Reference modulus, 12.0×10^6 psi

Case B

$E_r = E$

$E_\theta = 1.01E$

A

A $E_\theta = .99E$
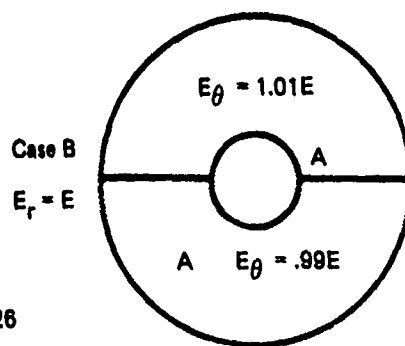
97-726

Figure 3–12. 2-D Models used to evaluate asymmetric property variations.

SECTION 4

ANALYSIS OF STATIC SIMULATION TEST

4.1 INTRODUCTION

The purpose of this investigation is to attempt to design a static test that will simulate the flywheel stress conditions that would be encountered under inertial loading in practice. Such a test would of course greatly expedite the development of bi-directionally reinforced flywheels by avoiding the problems associated with dynamic testing and by allowing test specimens to be thinner and/or smaller than a full scale flywheel and thus save on fabrication costs.

As a starting point we will seek to develop a test configuration that will simulate the stress components σ_r, σ_θ, σ_{rz}, and $\sigma_{r\theta}$ shown in Table 1-1. The 2-D and equivalent axisymmetric results shown in Table 1-1 are very similar, and we shall pick as a starting point those given by the equivalent axisymmetric analysis because it was used originally to design the wheel. Expressing these stresses in relative terms gives the following:

$$\sigma_r / \sigma_\theta = 1.0 \tag{4-1}$$

$$\sigma_{rz} / \sigma_\theta = .00777 \tag{4-2}$$

$$\sigma_{r\theta} / \sigma_\theta = .01903 \tag{4-3}$$

It should be pointed out that these ratios do not occur simultaneously in the original flywheel because σ_r and σ_θ do vary with the local radius r. However, as a first cut at the simulation problem it seems reasonable to seek a simulation as close as possible to the relative values cited above.

The strategy used to find a configuration which simulates the three stress ratios is similar to that used to design the original flywheel. First equivalent "smeared out" axisymmetric analyses and other simplified analyses are carried out to obtain geometric configurations approximately simulating the desired stress ratios. As in the flywheel design, the $E_{90} = 0$ assumption is carried along to simulate a crazed condition. After this, a two dimensional finite element analysis is carried out to verify the design.

4.2 GEOMETRIC PARAMETERS

The geometric parameters available in the simulation test shown in Figure 4-1 are:

N_r The number of radials per layer

R_{in}, R_{out} The inside and outside radii of the hoops

$$\frac{\hat{h}_r}{\hat{h}_\theta} = 1 - \frac{r_{in}}{r}$$

$R_{out} = 9.75$

$R_{in} = 1.625$

97-727
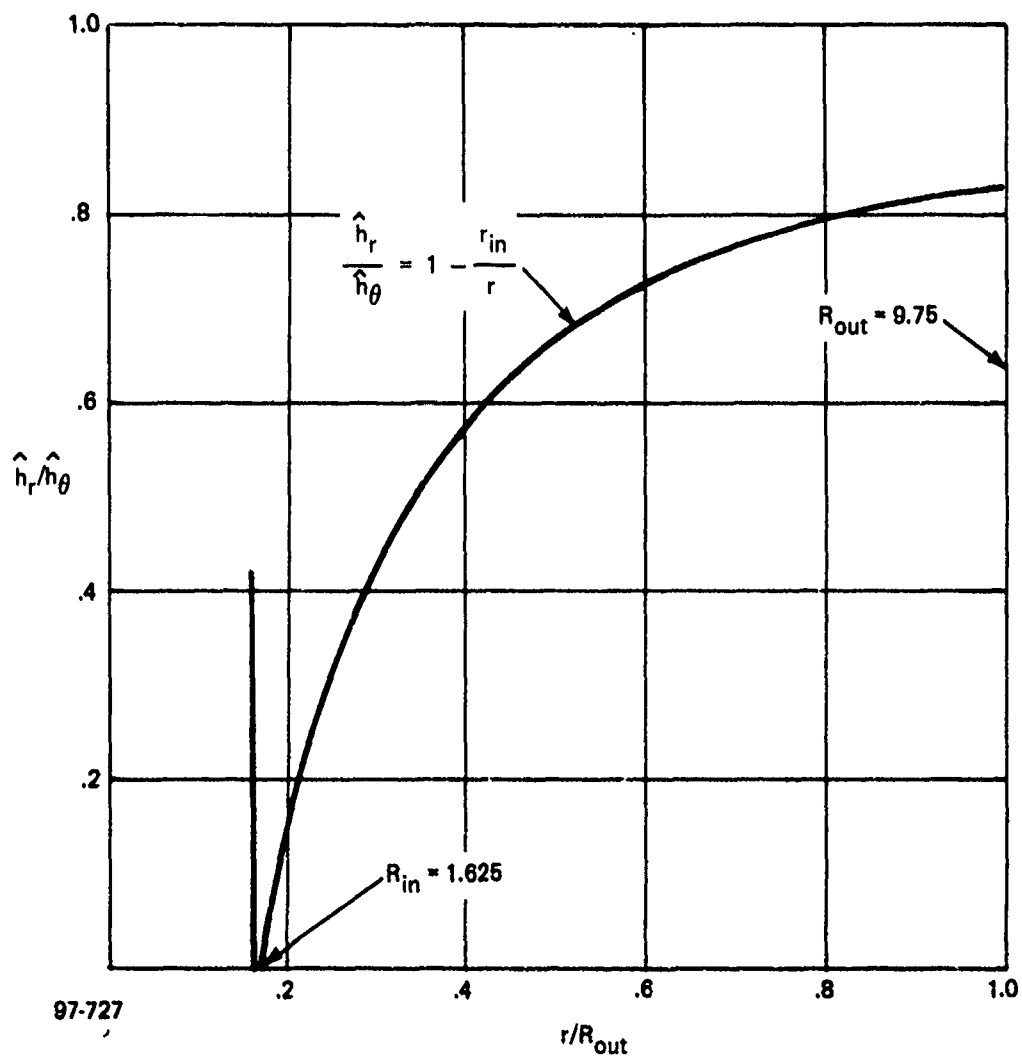
Figure 4—1. Ideal variation of equivalent radial thickness $\hat{h}_r$ for static simulation test.

-52-

| H_r, H_θ | The radial and hoop thicknesses (actual) |
| $\gamma(r)$ | The portion of the circumference at a given radius r occupied by radials. |

The ratio of internally applied load to externally applied load is also a parameter. However, for the initial part of this investigation the internal pressure is assumed to be zero.

For analytical purposes it is convenient to introduce two more parameters as follows:

| $\hat{h}_r(r)$ | "smeared out" radial thickness, averaged with respect to variations with θ |
| $\hat{h}_\theta(r)$ | "smeared out" hoop thickness, analogous to $h_r(r)$. |

In this work, we consider only the case of uniformly thick hoop layers such that $\hat{h}_\theta = H_\theta$.

4.3 SIMULATION OF $\sigma_r/\sigma_\theta = 1$

Ideal Shape

For the equivalent "smeared out" axisymmetric model with $E_{90} = 0$, it is possible to solve for $\hat{h}_r(r)$, the equivalent radial thickness for which $\sigma_r/\sigma_\theta = 1$ throughout the region $R_{in} < r < R_{out}$.

Under these assumptions the equation of equilibrium for the case $\sigma_r = \sigma_\theta$ and $\Omega = 0$ (no inertial force) is:

$$-\sigma\,\hat{h}_\theta + \sigma\,\hat{h}_r + \sigma r\,\frac{d\hat{h}_r}{dr} = 0 \qquad (4\text{-}4)$$

where $\hat{h}_\theta$ is the thickness of the hoop layer, which is constant with respect to r.

The solution of this equation subject to a force free inner boundary condition of $\sigma \cdot \hat{h}_r = 0$ which becomes $\hat{h}_r = 0$, is the following:

$$\frac{\hat{h}_r}{\hat{h}_\theta} = 1 - \frac{R_{in}}{r} \qquad (4\text{-}5)$$

A plot of this equation is given in Figure 4-1.

Unfortunately, this ideal shape leads to infinitely high interlaminar shear stresses, σ_{rz}, between the hoops and radials at the inside edge ($r = R_{in}$). This comes about in the following way. First, from Equation (4-5) one

-53-

has $\hat{h}_r = 0$ when $r = R_{in}$. Second, from the definition of the "smearing out", the width of a radial (i.e., in θ direction), $W(r)$, is given by:

$$W(r) = \frac{2\pi r}{N_r H_r} \cdot \hat{h}_r(r)$$

Consequently, at the inside edge ($r = R_{in}$), the radial width is zero. Thus, as one approaches the inside edge ($r \to R_{in}$) the area for load transfer between hoop and radial reinforcements approaches zero and infinitely high interlaminar shear stresses arise. This effect can also be deduced from Equation (4-14).

Solution for Constant $\hat{h}_r$

This problem was solved in the case of the wheel by increasing h_r near the inside edge, i.e., by adding "tabs." In the simulation we anticipate the case of a relatively narrow ring ($R_{out}-R_{in}$ is small) and therefore seek a configuration like that shown in Figure 4-2 where the radials occupy a constant angular portion of the wheel. This analytical model can be solved by solving the equation

$$-\sigma_\theta \hat{h}_\theta + \sigma_r \hat{h}_r + r \frac{d\sigma_r}{dr} \hat{h}_r = 0 \tag{4-6}$$

where now $\hat{h}_r$ is a constant and σ_r and σ_θ are given by

$$\sigma_\theta = E \frac{W}{r} \tag{4-7}$$

$$\sigma_r = E \frac{\partial W}{\partial r} \tag{4-8}$$

The solution obtained by substituting σ_θ and σ_r into the equilibrium equation and invoking the boundary condition $\sigma_r = 0$ at $r = R_{in}$ is as follows:

$$\frac{\sigma_\theta}{\sigma} = \frac{1}{a} \frac{\left[\left(\dfrac{R_{in}}{R_{out}}\right)^{-2a}\left(\dfrac{r}{R_{out}}\right)^{a-1} + \left(\dfrac{r}{R_{out}}\right)^{-a-1}\right]}{\left[\left(\dfrac{R_{in}}{R_{out}}\right)^{-2a} - 1\right]} \tag{4-9}$$
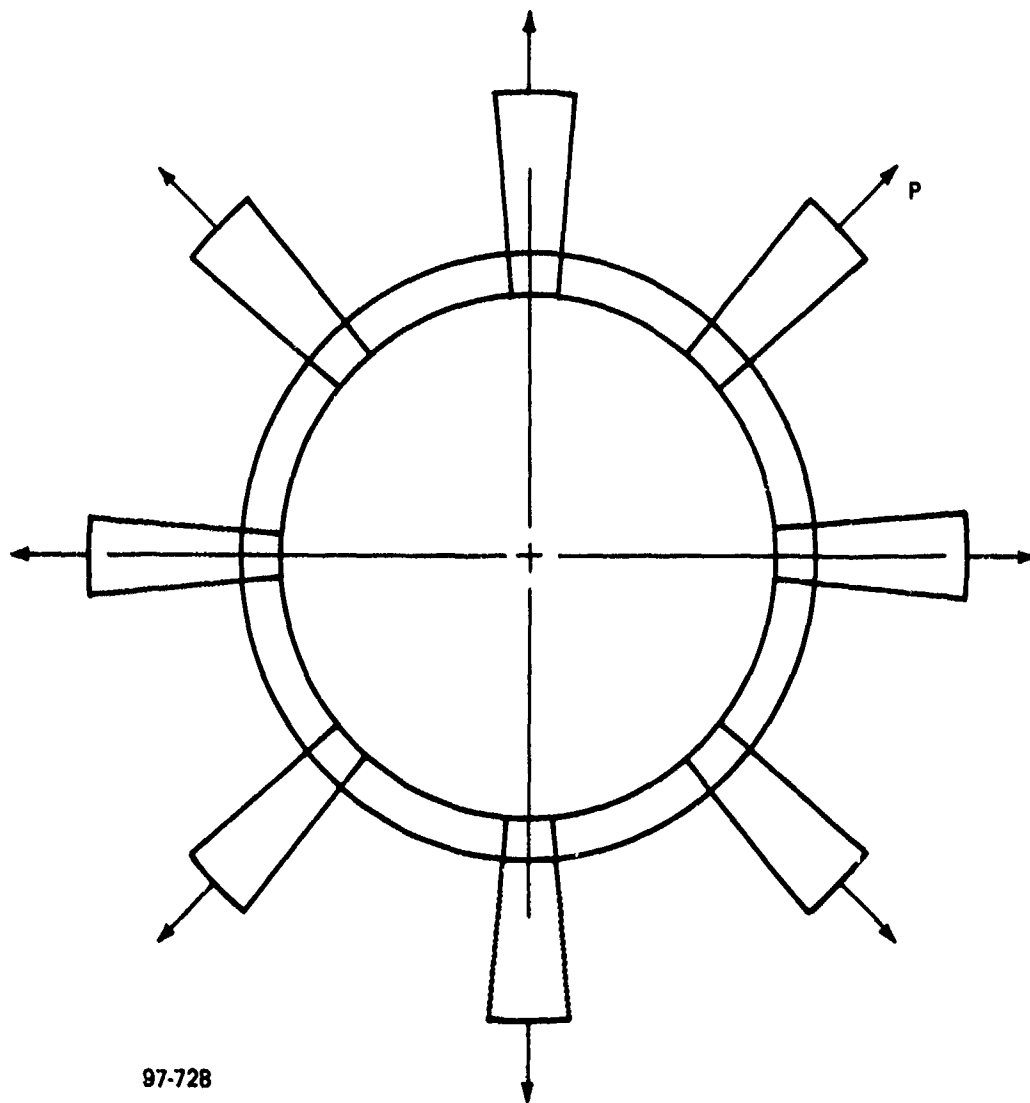
97-728

Figure 4—2. Schematic of static simulation test.

and

$$\frac{\sigma_r}{\sigma} = \frac{\left[\left(\frac{R_{in}}{R_{out}}\right)^{-2a} \left(\frac{r}{R_{out}}\right)^{a-1} - \left(\frac{r}{R_{out}}\right)^{-a-1}\right]}{\left[\left(\frac{R_{in}}{R_{out}}\right)^{-2a} - 1\right]} \qquad (4\text{-}10)$$

where σ is the value of σ_r at the outside radius $r = R_{out}$ and a is given by

$$a = \sqrt{\frac{\hat{h}_\theta}{\hat{h}_r}} \qquad (4\text{-}11)$$

It is desired to pick a ratio $\hat{h}_r/\hat{h}_\theta$ such that the maximum values of σ_r and σ_θ are equal. A plot giving the desired ratios $\hat{h}_r/\hat{h}_\theta$ as determined from the above formulas is given in Figure 4-3.

Hoop Bending Effects

If the radials shown in Figure 4-2 are too far apart, then the hoop ring will undergo bending and the values of σ_r and σ_θ will deviate from those predicted from the equivalent "smeared out" axisymmetric analysis. Although this problem is negligible in the actual flywheel where N_r (number of radials) and $R_{out}-R_{in}$ are large it is of primary concern in a simulation test where it is desirable to keep N_r as low as possible for practical and cost reasons.

This effect was evaluated parametrically by solving Flügge's ring equations* for the case of a simplified ring model where the radial loads are assumed to be applied as point loads at the position of each radial centerline. This analysis is expected to overestimate the effects caused by bending and provide a conservative method for excluding simulation tests designs with insufficient numbers of radials. Applying Flügge's equations and solving for the moment M_0 in the ring at the point of load application gives

$$M_0 = \frac{1}{\hat{\theta}}\left[Q_0 \hat{R} (\cos\hat{\theta} - 1) + N_0 \hat{R} (\hat{\theta} - \hat{\theta} \sin\hat{\theta})\right] \qquad (4\text{-}12)$$

where

$\hat{\theta}$ = polar angle between centerline of radial and middle point between radials.

$\hat{R}$ = average radius of the hoop ring

---

*Flügge, W., Stresses in Shells, Springer-Verlag, Berlin, 1960.
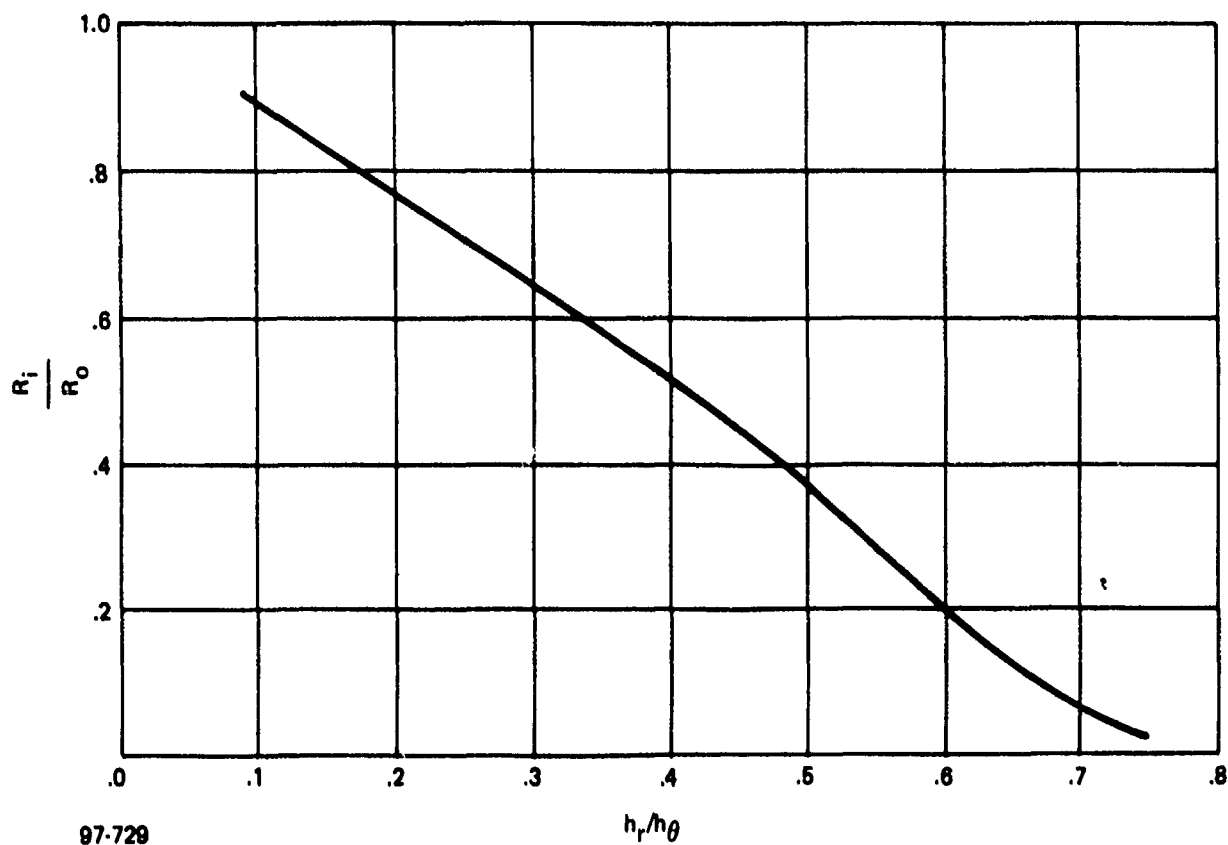
Figure 4–3. Ratios of $\hat{h}_r/\hat{h}_\theta$ for which $\sigma_{r_{max}} = \sigma_{\theta_{max}}$ (for constant h_r)

Q_o = shear force at centerline of radial (equals on half of total radial load)

N_o = hoop membrane force.

It was found that M_o is greater in absolute magnitude than the bending moment midway between radials. Computing the bending stress due to M_o and comparing it to the hoop stress associated with N_o leads to the design plot shown in Figure 4-4. The asymptotic formula for small θ is

$$\frac{\sigma_{bending}}{\sigma_{hoop}} = \left[1 + \frac{2 \hat{R} \hat{\theta}^2}{(R_{out} - R_{in})} \right] \tag{4-13}$$

It can be seen from Figure 4-4 that if a typical case of $R_{out}-R_{in}$ = 1 inch is taken, then approximately 25 radials (N_r = 25) are required to keep the bend stresses below 5 percent of the hoop stresses.

It turns out, however, that the restrictions implied by Figure 4-4 are less severe than those required to simulate the condition $\sigma_{r\theta}/\sigma_\theta$ = .01903.

4.4 SIMULATION OF $\sigma_{rz}/\sigma_\theta$ = .00777

The derivation used to compute σ_{rz} and $\sigma_{r\theta}$ for the equivalent "smeared out" axisymmetric analysis is shown schematically in Figure 4-5. The equations are obtained by taking free body diagrams of EFCD and ABCD, respectively. The assumption E_{90} = 0 precludes the possibility of any radial stresses σ_r on the surfaces FC or ED of the hoop layers. These surfaces can contain very small amounts of shear stress, but as indicated by the more detailed 2-D finite element analyses they act almost perpendicular to the radial direction used in summing forces and are negligible. The factor of 2 in the equation for σ_{rz} average is caused by the fact that the load is transferred from two sides of each hoop layer. As in the design of the flywheel, this has serious implications for layers adjacent to the outside edge ($Z = Z_{max}$) of the flywheel. In the flywheel design, an extra wide set of radials was used just inside the outermost hoop layer to maintain similar levels of σ_{rz} stress near the outside. For the simulation it appears more appropriate to put a set of radials one half the usual thickness on the outside so that the σ_{rz} stresses do not vary from layer to layer.

Working out the geometry indicated in the equations of Figure 4-5 leads to the following:

$$\sigma_{rz_{ave.}} = \frac{-h_\theta}{2 r \gamma} \sigma_\theta \tag{4-14}$$
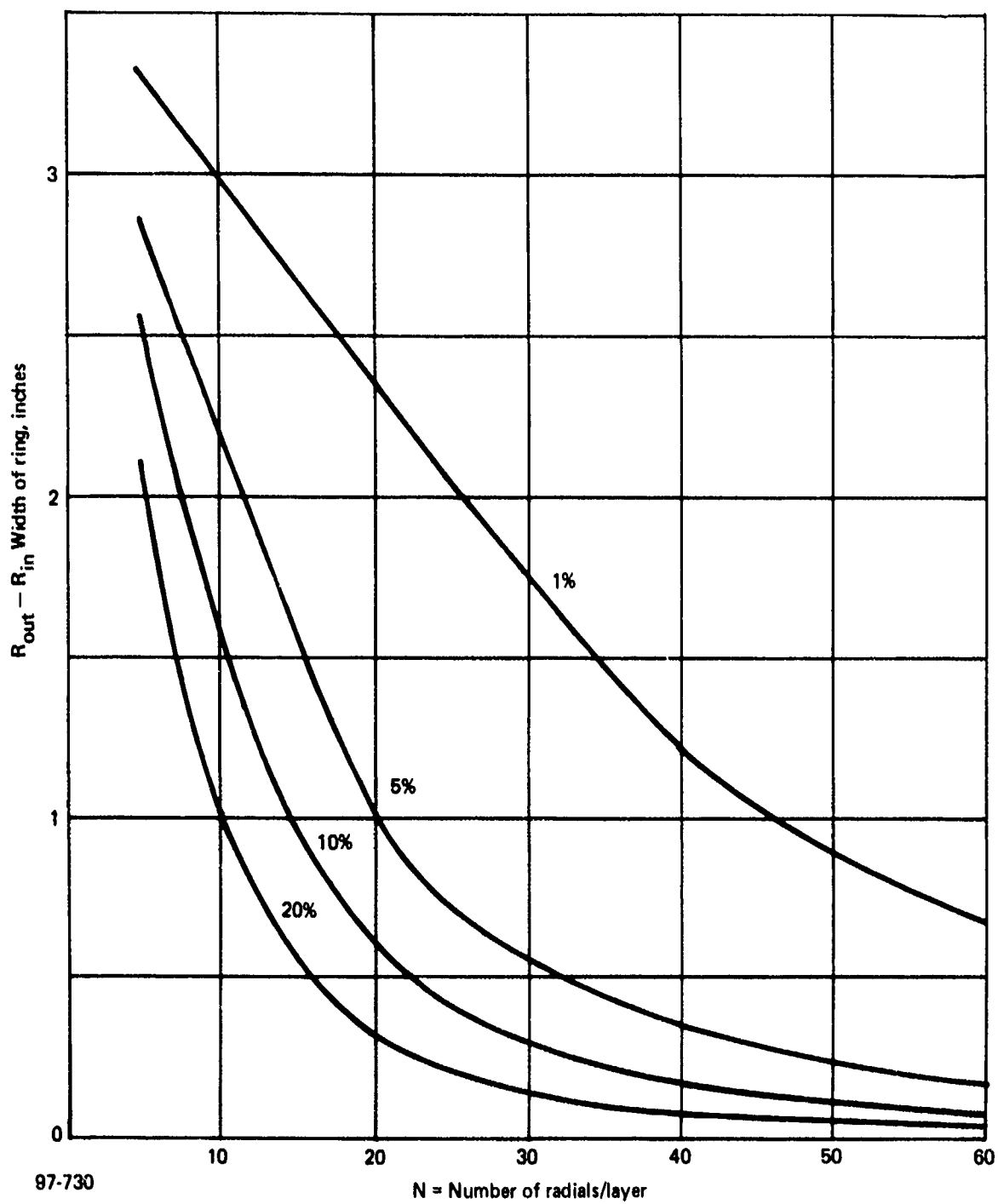
Figure 4—4. Percent change in hoop stress caused by local bending.
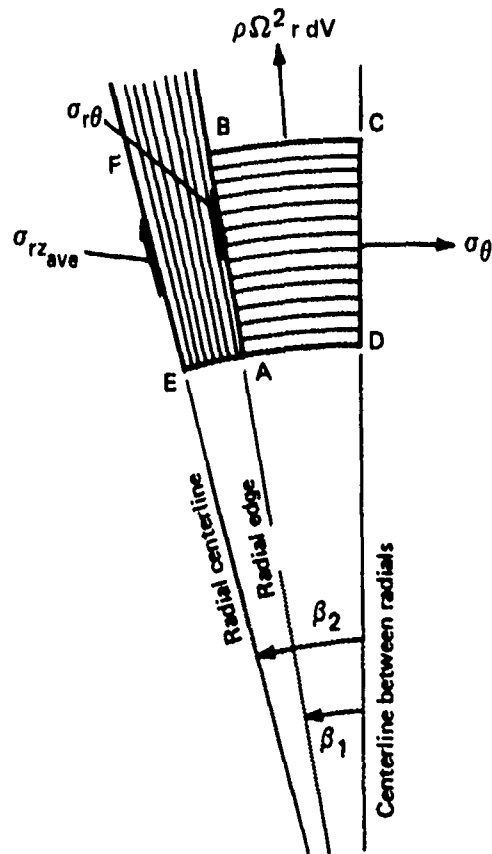
Summing forces in local radial directions gives

$$\sigma_{rz_{ave}} \times 2 \times \text{AREA (AEFB)} = \beta_2 \cdot \text{DC} \cdot h_\theta \cdot \sigma_\theta$$

$$\sigma_{r\theta} \cdot h_\theta \cdot \text{AB} = \beta_1 \, (\rho\Omega^2 r^2 - \sigma_\theta) \cdot h_\theta \cdot \text{DC}$$

For static simulation $\Omega = 0$

97-731

Figure 4—5. Schematic of derivation of σ_{rz} and $\sigma_{r\theta}$ stresses.

where

r is the local radius

y is the local fraction of the circumference occupied by radials.

4.5 SIMULATION OF $\sigma_{r\theta}/\sigma_\theta = .01903$

Similar application of the equations shown in Figure 4-5 gives

$$\sigma_{r\theta} = -\frac{\pi}{N_r} \ (1-y)\,\sigma_\theta \tag{4-15}$$

where N_r is the number of radials.

As we shall see in the subsequent section, this last equation places the most severe restraint on the minimum acceptable number of radials, N_r.

4.6 SELECTION OF A TYPICAL SIMULATED FLYWHEEL CONFIGURATION

We next apply the relationship developed in Sections 4.1 through 4.5 to define a simulation test.

In order to satisfy Equation (4-15) a tradeoff must be made between the dual evils of too many radials on the one hand and too large a y, the relative area occupied by radials, on the other. Our mutual selection, satisfying Equations (4-15) and (4-3), is:

$N_r = 48$

$y = .7092$

If we select $R_{in} = 1.625 =$ same as flywheel, then the circumferential distance between radials centerlines is .2127. The areas between radial centerlines are then kept roughly square by selecting $R_{out} - R_{in} = .25$ inch. For this combination Equation (4-13) indicates an acceptable deviation from pure hoop stress of 6 percent. For this combination of R_{in}/R_{out}, Figure 4-3 indicates $h_r/h_\theta = .125$.

We next use Equations (4-14) and (4-2) to find $h_\theta = .0179$. Then for h_r we have .125 x .0179 = .0022 inch. The actual radial thickness $H_r = \hat{h}_r/y = .00310$. In summary, the resulting simulated configuration is:

Geometry Selected for Simulation Test

N_r = 49 radials/layer

y = .7092

R_{in} = 1.625

R_{out} = 1.875

H_r = .00310 actual radial thickness

$\hat{h}_r$ = .0022

$\hat{h}_\theta$ = .0179

If it is found impractical to fabricate the values of H_r and $\hat{h}_\theta$ cited above, one can merely scale up R_{in}, R_{out}, H_r and $\hat{h}_\theta$ until a more suitable combination is found, without altering the accuracy of the simulation.

SECTION 5

TESTING FOR DEGRADED PROPERTY EFFECTS

5.1 MECHANICAL EVALUATION

A biaxial tensile test was devised whereby the Kevlar 0° - 90° lay-up could be stressed in both directions simultaneously. Subsequent to this biaxial loading the stressed composite at the junction or overlap region was machined into samples for evaluation of shear properties after loading.

The method of testing in this series is a sandwich beam using a honey-comb core between an aluminum skin and a composite (test piece) skin. The loading method is essentially a double beam flexure test using four point loading on each leg. The schematic of this test is given in Figure 5-1. The samples are loaded at particular stress levels to simulate various flywheel speeds, i.e., 50, 60 and 70% of ultimate, and then off-loaded. The composite material is then removed from the sandwich structure and samples are fabricated from the areas at the $0^\circ/90^\circ$ overlaps. The samples are designed to obtain shear properties after biaxial loading. The tests selected are 45° tension for determining Young's modulus and Poisson's ratio (which could then be converted to shear modulus) and tensile and shear stress; and horizontal (short beam shear) to determine interlaminar shear stress. Figure 5-2 shows the areas and orientations of the test samples removed.

The matrix of tests to be performed in this series is given in Table 5-1.

TABLE 5-1. $0^\circ/90^\circ$ BEAM TEST (BIAXIAL TENSION)

Span (inch)	Load point separation (inch)	Load level (%)	Number of replicates
20	4	100	2
20	4	80	2
20	4	70	2
20	4	60	2

SUBSEQUENT COUPON TESTS ON COMPOSITE OVERLAP

Test	No. of replicates (each beam)	Data generated
45° tensile	1	45° , ν, G, E,
45°	2	(interlaminar)

P/4 **P/4**

P/4

P/4 **P/4**

P/4 **P/4**

4"

6061 T6 1/8"

5"

1/8" Cell aluminum honeycomb

2"

20"

Kevlar composite

97-731

A – A
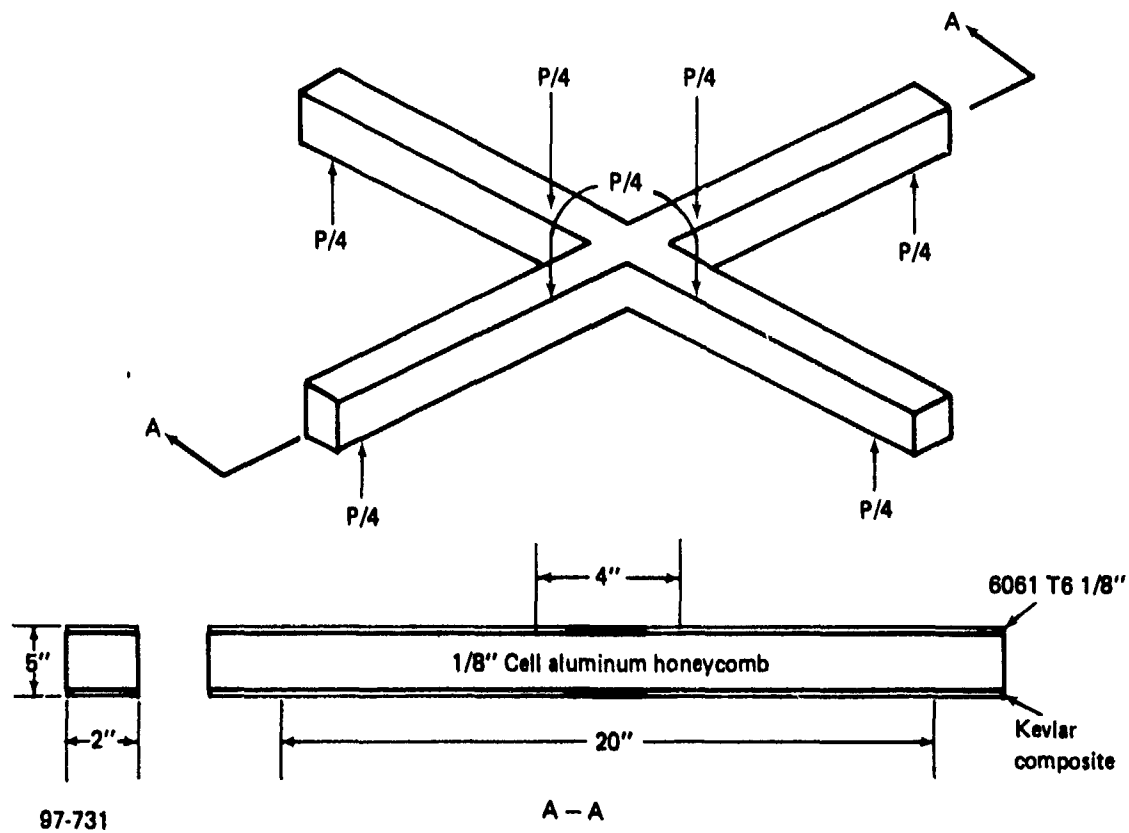
Figure 5–1. Biaxial beam schematic.
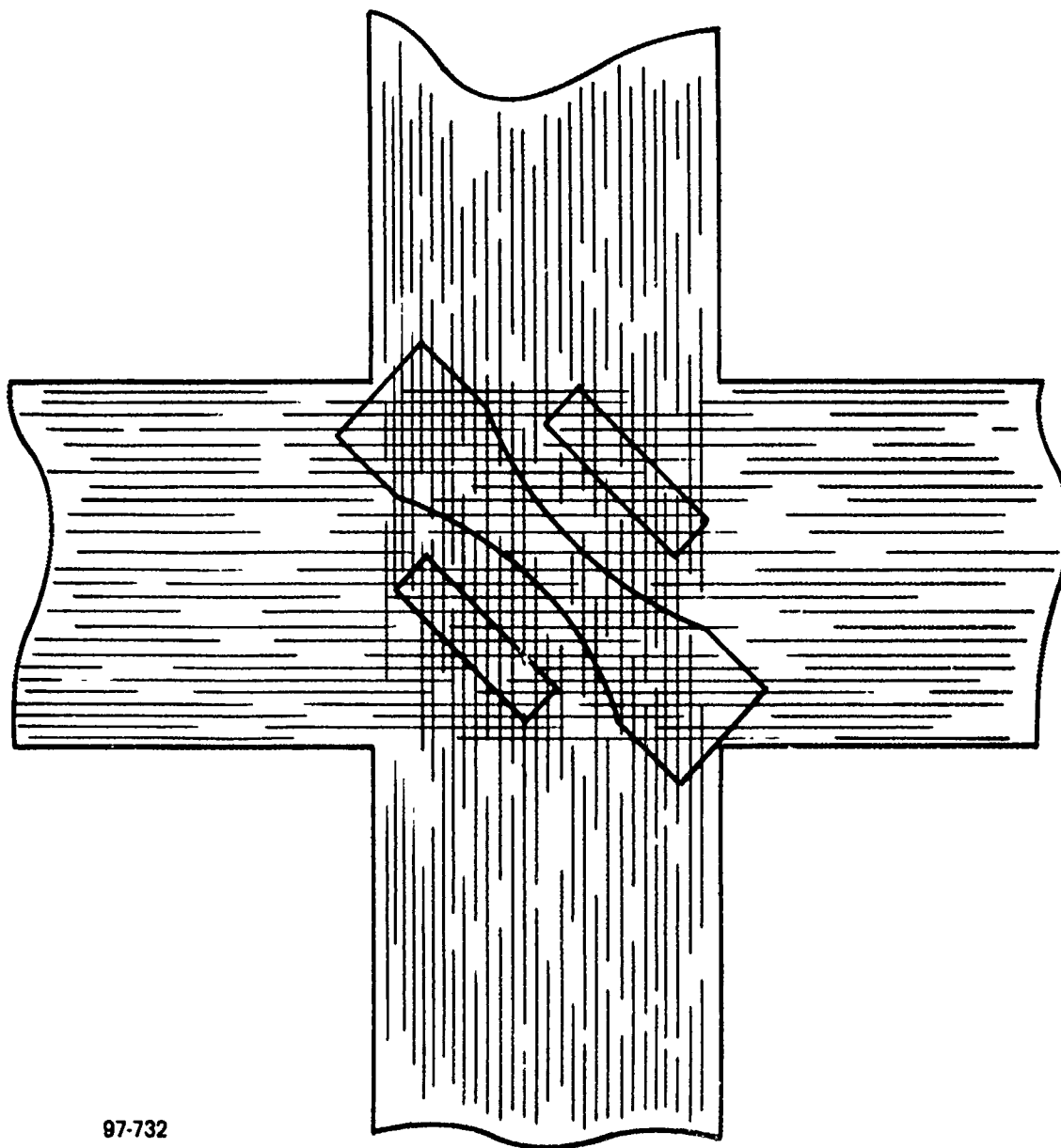
97-732

Figure 5—2. Coupon sample layout for subsequent tensile and short beam shear tests.

5.2 COMPOSITE LAY-UP

Since there was an abundance of 9 inch long uni-directional prepreg Kevlar epoxy on hand at the outset of this test series, and since there was a waiting period for receipt of any roll goods which were on order, it was decided to go along and fabricate the first two beams with 9 inch strips layed up with overlap and butt joints. The remaining beams in the series, however, are made with 22 inch strips of uni-directional Kevlar layed up at 0° and 90° alternating angles. Also, the first two beams contain 2 plies of composite in each direction for a total of 4 plies whereas the remaining samples are constructed with 3 plies in each direction. Figure 5-3 is an attempt to depict the butt and overlap joint sequence herewith described.

5.3 REDUCTION OF DATA

At the time of this writing, one* test has been carried out at 52 percent of ultimate load. From these tests the following average properties were obtained:

$$E_{45^\circ} = .99 \times 10^6 \text{ psi}$$

$$\sigma_{ultimate} = 5750 \text{ psi}$$

The next step is to derive from these quantities the quantities G_{12} and σ_{12} allowable. The modulus G_{12} is obtained from the transformation laws and is

$$G_{12} = \frac{1}{\dfrac{4}{E_{45}} - \dfrac{2}{E_1}}$$

which gives $G_{12} = .25 \times 10^6$. The state of stress at a 45° orientation from the direction of loading is given by

$$\sigma_1 = \sigma_2 = \sigma_{12} = \frac{\sigma}{2}$$

Tsai-Hill Failure criterion then gives

$$\left(\frac{\sigma_1}{X}\right)^2 - \frac{\sigma_1 \sigma_2}{X^2} + \left(\frac{\sigma_2}{Y}\right)^2 + \left(\frac{\tau_{12}}{S}\right)^2 = 1$$

---

*A second biaxial test failed and prevented measurement of the degraded modulus.
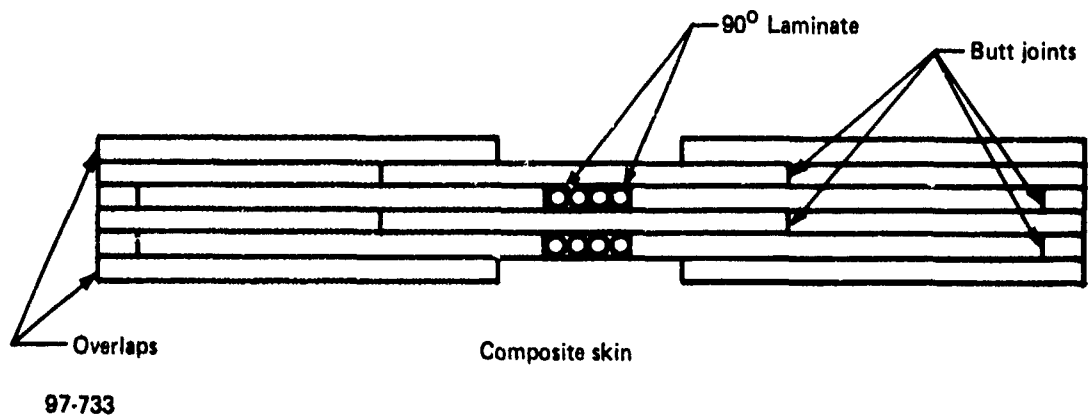
Figure 5-3. Butt joints and overlap scheme for 9-inch long strips.

which reduces to:

$$\left(\frac{\sigma}{2Y}\right)^2 + \left(\frac{\sigma}{2S}\right)^2 = 1$$

Since for Kevlar 49 the undegraded shear strength S is much lower than the 0° strength Y we have

$$S = \frac{\sigma}{2} = 5750$$

Tabulating the results gives

Quantity	Undegraded	Degraded	Ratio of degraded/undegraded
G_{12}	$.3 \times 10^6$ psi	$.25 \times 10^6$	72.8%
σ_{12} allowable	7.9 ksi	5.75 ksi	82.5%

These results are then introduced into the analysis of Section 2 to evaluate the effects of degraded properties on flywheel performance.

SECTION 6

CONCLUSIONS

Structural analyses and experiments have been carried out to further the development of bi-directionally reinforced flywheels. A brief summary of the findings are presented.

1. The analysis indicates that for the biaxial stress levels used in the testing that shear modulus and strength degradations would not give rise to negative stress margins. In addition, the analytical results show that reductions in in-plane shear modulus of up to 90 percent have a small effect on the maximum 0° stresses.

2. The efficiency of a bi-directionally reinforced flywheel is sensitive to variations in fiber volume, and variations in hoop and radial reinforcement geometry. The relationship between variations in efficiency and variations in property and geometric inputs differ from case to case and are presented in detail in the report. Asymmetric variations in material properties can also lead to substantial wheel imbalances which depend on the degree on nonuniformity present.

3. Static simulation tests appear feasible but must include a sufficient number of radials to prevent premature shear failures.

4. Biaxially degraded property effects have been obtained from crossbeam sandwich tests and subsequent 45° tensile tests and the resulting data input into the analysis.

No. of Copies	To	No. of Copies	To

1 Office of the Director, Defense Research and Engineering, The Pentagon, Washington, D. C. 20301

12 Commander, Defense Documentation Center, Cameron Station, Building 5, 5010 Duke Street, Alexandria, Virginia 22314

1 Metals and Ceramics Information Center, Battelle Columbus Laboratories, 505 King Avenue, Columbus, Ohio 43201

Deputy Chief of Staff, Research, Development, and Acquisition, Headquarters Department of the Army, Washington, D. C. 20310
1 ATTN: DAMA-ARZ

Commander, Army Research Office, P.O. Box 12211, Research Triangle Park, North Carolina 27709
1 ATTN: Information Processing Office

Commander, U. S. Army Materiel Development and Readiness Command, 5001 Eisenhower Avenue, Alexandria, Virginia 22333
1 ATTN: DRCLDC, Mr. R. Zentner

Commander, U. S. Army Communitions Research and Development Command, Fort Monmouth, New Jersey 07703
1 ATTN: DRDCO-GG-TD
1   DRDCO-GG-DM
1   DRDCO-GG-E
1   DRDCO-GG-EA
1   DRDCO-GG-ES
1   DRDCO-GG-EG

Commander, U. S. Army Missile Research and Development Command, Redstone Arsenal, Alabama 35809
1 ATTN: Technical Library
1   DRSMI-RSM, Mr. E. J. Wheelahan

Commander, U. S. Army Natick Research and Development Command, Natick, Massachusetts 01760
1 ATTN: Technical Library
1   Dr. E. W. Ross
1   DRDNA-UE, Dr. L. A. McClaine

Commander, U. S. Army Satellite Communications Agency, Fort Monmouth, New Jersey 07703
1 ATTN: Technical Document Center

Commander, C. S. Army Tank-Automotive Research and Development Command, Warren, Michigan 48090
1 ATTN: DRDTA-RKA
1   DRDTA, Technical Library

Commander, U. S. Army Armament Research and Development Command, Rock Island, Illinois 61201
1 ATTN: Technical Library

Commander, White Sands Missile Range, New Mexico 88002
1 ATTN: STEWS-WS-VT

Commander, Aberdeen Proving Ground, Maryland 21005
1 ATTN: STEAP-TL, Bldg. 305

Commander, Frankford Arsenal, Philadelphia, Pennsylvania 19137
1 ATTN: Library, H1300, Bl. 51-2

Commander, U. S. Army Ballistic Research Laboratory, Aberdeen Proving Ground, Maryland 21005
1 ATTN: Dr. J. Frasier
:   Dr. R. Vitali
1   Dr. G. L. Filbey
1   Dr. R. Karpp
1   Dr. W. Gillich

Commander, Harry Diamond Laboratories, 2300 Powder Mill Road, Adelphi, Maryland 20783
1 ATTN: Technical Information Office

Commander, Picatinny Arsenal, Dover, New Jersey 07801
1 ATTN: SARPA-RT-S
1   Mr. A. Devine
1   Mr. A. M. Anzalone, SARPA-FR-M-D, PLASTEC

Commander, Redstone Scientific Information Center, U. S. Army Missile Command, Redstone Arsenal, Alabama 35809
1 ATTN: DRSMI-R8LD, Document Section

Commander, Watervliet Arsenal, Watervliet, New York 12189
1 ATTN: Dr. T. Davidson
1   Mr. D. P. Kendall
1   Mr. J. F. Throop
1   SARWV-RDR, Dr. F. W. Schmiedeshoff

Commander, U. S. Army Foreign Science and Technology Center, 220 7th Street, N. E., Charlottesville, Virginia 22901
1 ATTN: Mr. Marley, Military Technologies

Commander, U. S. Army Aeromedical Research Unit, P. O. Box 577, Fort Rucker, Alabama 36460
1 ATTN: Technical Library

Director, Eustis Directorate, U. S. Army Air Mobility Research and Development Laboratory, Fort Eustis, Virginia 23604
1 ATTN: Mr. J. Robinson, DAVDL-E-MOS (AVRADCOM)
1   Mr. R. Berresford

U. S. Army Aviation Training Library, Fort Rucker, Alabama 36362
1 ATTN: Bldg. 5906-5907

Commander, U. S. Army Board for Aviation Accident Research, Fort Rucker, Alabama 36360
1 ATTN: Library, Bldg. 5505

Commander, USACDC Air Defense Agency, Fort Bliss, Texas 79916
1 ATTN: Technical Library

Commander, U. S. Army Engineer School, Fort Belvoir, Virginia 22060
1 ATTN: Library

Commander, U. S. Army Engineer Waterways Experiment Station, Vicksburg, Mississippi 39180
1 ATTN: Research Center Library

Commander, Naval Air Engineering Center, Lakehurst, New Jersey 08733
1 ATTN: Technical Library, Code 115

Naval Air Development Center, Aero Materials Department, Warminster, Pennsylvania 18974
1 ATTN: J. Viglione

David Taylor Naval Ship Research and Development Laboratory, Annapolis, Maryland 21402
1 ATTN: Dr. H. P. Chu

Naval Underwater Systems Center, New London, Connecticut 06320
1 ATTN: R. Kasper

Naval Research Laboratory, Washington, D. C. 20375
1 ATTN: C. D. Beachem, Head, Adv. Mat'ls Tech. Br., Code 6310
1   Dr. J. M. Krafft - Code 8430

Chief of Naval Research, Arlington, Virginia 22217
1 ATTN: Code 471

Naval Weapons Laboratory, Washington, D. C. 20390
1 ATTN: H. W. Romine, Mail Stop 103

Director, Structural Mechanics Research, Office of Naval Research, 800 North Quincy Street, Arlington, Virginia 22203
1 ATTN: Dr. N. Perrone

No. of Copies	To	No. of Copies	To

No. of Copies	To
1	Ship Structure Committee, Maritime Transportation Research Board, National Research Council, 2101 Constitution Avenue, N. W., Washington, D. C. 20418
	Air Force Materials Laboratory, Wright-Patterson Air Force Base, Ohio 45433
1	ATTN: AFML (MXE), E. Morrissey
1	AFML (LC)
1	AFML (LLP), D. M. Forney, Jr.
1	AFML (LNC), T. J. Reinhart
1	AFFDL/FB, Dr. J. C. Halpin
1	AFML (MBC), Mr. Stanley Schulman
1	Dr. S. Tsai
1	Dr. N. Pagano
	Air Force Flight Dynamics Laboratory, Wright-Patterson Air Force Base, Ohio 45433
1	ATTN: AFFDL (FBS), C. Wallace
1	AFFDL (FBE), C. D. Sendeckyj
	National Aeronautics and Space Administration, Washington, D. C. 20546
1	ATTN: Mr. B. G. Achhammer
1	Mr. G. C. Deutsch - Code RW
	National Aeronautics and Space Administration, Marshall Space Flight Center, Huntsville, Alabama 35812
1	ATTN: R. J. Schwinghamer, EH01, Dir., M&P Lab
1	Mr. W. A. Wilson, EH41, Bldg. 4612
	National Aeronautics and Space Administration, Langley Research Center, Hampton, Virginia 23665
1	ATTN: Mr. H. F. Hardrath, Mail Stop 188M
1	Mr. R. Foye, Mail Stop 188A
	National Aeronautics and Space Administration, Lewis Research Center, 21000 Brook Park Road, Cleveland, Ohio 44135
1	ATTN: Mr. S. S. Manson
1	Dr. J. E. Srawley, Mail Stop 105-1
1	Mr. W. F. Brown, Jr.
	Panametrics, 221 Crescent Street, Waltham, Massachusetts 02154
1	ATTN: Mr. K. A. Fowler
	Wyman-Gordon Company, Worcester, Massachusetts 01601
1	ATTN: Technical Library
	Lockheed-Georgia Company, 86 South Cobb Drive, Marietta, Georgia 30063
1	ATTN: Materials & Processes Eng. Dept. 71-11, Zone 54
	National Bureau of Standards, U. S. Department of Commerce, Washington, D. C. 20234
1	ATTN: Mr. J. A. Bennett
1	Mechanical Properties Data Center, Belfour Stulen Inc., 13917 W. Bay Shore Drive, Traverse City, Michigan 49684
1	Mr. W. F. Anderson, Atomics International, Canoga Park, California 91303
	Midwest Research Institute, 425 Coker Boulevard, Kansas City, Missouri 64110
1	ATTN: Mr. C. Q. Bowles
1	Dr. J. Charles Grosskreutz, Asst. Dir. for Research, Solar Energy Research Institute, 1536 Cole Boulevard, Golden, Colorado 80401
1	Mr. A. Hurlich, Convair Div., General Dynamics Corp., Mail Zone 630-01, P.O. Box 80847, San Diego, California 92138
	Virginia Polytechnic Institute and State University, Dept. of Eng. Mechanics, 230 Norris Hall, Blacksburg, Virginia 24061
1	ATTN: Prof. R. M. Barker
1	Assoc. Prof. G. W. Swift
	Southwest Research Institute, 8500 Culebra Road, San Antonio, Texas 78284
1	ATTN: Mr. G. C. Grimes

No. of Copies	To
	IIT Research Institute, Chicago, Illinois 60616
1	ATTN: Dr. I. M. Daniel
1	Mr. J. G. Kaufman, Alcoa Research Laboratories, New Kensington, Pennsylvania 15068
1	Mr. G. M. Orner, MANLABS, 21 Erie Street, Cambridge, Massachusetts 02139
1	Mr. P. N. Randall, TRW Systems Group - 0-1/2210, One Space Park, Redondo Beach, California 90278
1	Dr. E. A. Steigerwald, TRW Metals Division, P.O. Box 250, Minerva, Ohio 44657
1	Mr. W. A. Van der Sluys, Research Center, Babcock and Wilcox, Alliance, Ohio 44601
1	Mr. B. M. Wundt, 2346 Shirl Lane, Schenectady, New York 12309
	Battelle Columbus Laboratories, 505 King Avenue, Columbus, Ohio 43201
1	ATTN: Dr. E. Rybicki
1	Dr. K. R. Merckx, Battelle Northwest Institute, Richland, Washington 99352
	General Electric Company, Schenectady, New York 12010
1	ATTN: Mr. A. J. Brothers, Materials and Processes Laboratory
	General Electric Company, Knolls Atomic Power Laboratory, P. O. Box 1072, Schenectady, New York 12301
1	ATTN: Mr. F. J. Mehringer
1	Mr. L. F. Coffin, Room 1C41-K1, Corp. R&D, General Electric Company, P.O. Box 8, Schenectady, New York 12301
1	Dr. A. K. Shoemaker, Research Laboratory, Mail Stop 78, United States Steel Corp., Monroeville, Pennsylvania 15146
	Westinghouse Electric Company, Bettis Atomic Power Laboratory, P. O. Box 109, West Mifflin, Pennsylvania 15122
1	ATTN: Mr. M. L. Parrish
	Westinghouse R&D Center, 1310 Beulah Road, Pittsburgh, Pennsylvania 15235
1	ATTN: Mr. E. T. Wessel
1	Mr. M. J. Manjoine
	Brown University, Providence, Rhode Island 02912
1	ATTN: Prof. J. R. Rice
1	Prof. W. N. Findley, Division of Engineering, Box D
	Carnegie-Mellon University, Department of Mechanical Engineering, Schenley Park, Pittsburgh, Pennsylvania 15213
1	ATTN: Dr. J. L. Swedlow
1	Prof. J. Dvorak, Chemical Engineering Department, Duke University, Durham, North Carolina 27706
	George Washington University, School of Engineering and Applied Sciences, Washington, D. C. 20052
1	ATTN: Dr. H. Liebowitz
	Lehigh University, Bethlehem, Pennsylvania 18015
1	ATTN: Prof. G. C. Sih
1	Prof. F. Erodgan
1	Dr. George R. Irwin, Department of Mechanical Engineering, University of Maryland, College Park, Maryland 20742
	Massachusetts Institute of Technology, Cambridge, Massachusetts 02139
1	ATTN: Prof. T. H. H. Pian, Department of Aeronautics and Astronautics
1	Prof. F. J. McGarry
1	Prof. A. S. Argon, Room 1-306
1	Prof. R. Greif, Dept. of Mech. Eng., Tufts University, Medford, Massachusetts 02155

No. of Copies	To
1	Dr. D. E. Johnson, AVCO Systems Division, Wilmington, Massachusetts 01887
1	Prof. B. Pipes, Dept. of Mech. Eng., Drexel University, Philadelphia, Pennsylvania 19104
1	Dr. A. S. Tetelman, Failure Analysis Associates, 11777 Mississippi Ave., Suite 4, Los Angeles California 90025
1	Prof. W. Goldsmith, Dept. of Mech. Eng., University of California, Berkeley, California 94720
1	Prof. A. J. McEvily, Metallurgy Dept U-136, University of Connecticut, Storrs, Connecticut 06268
1	Prof. D. Drucker, Dean of School of Engineering, University of Illinois, Champaign, Illinois 61820
1	University of Illinois, Urbana, Illinois 61820 ATTN: Prof. H. T. Corten, Dept. of Theoretical and Applied Mechanics, 212 Talbot Laboratory
1	Dr. M. L. Williams, Dean of Engineering, 240 Benedum Hall, University of Pittsburgh, Pittsburgh, Pennsylvania 15261
1	Prof. A. Kobayashi, Dept. of Mechanical Engineering, FU-10, University of Washington, Seattle, Washington 98195
1	Mr. W. A. Wood, Baillieu Laboratory, University of Melbourne, Melbourne, Australia

No. of Copies	To
1	Mr. Elmer Wheeler, Airesearch Manufacturing Company, 402 S. 36th Street, Phoenix, Arizona 85034
1	Mr. Charles D. Roach, U.S. Army Scientific and Technical Information Team, 6000 Frankfurt/Main, I.G. Hochhaus, Room 750, West Germany (APO 09710, NY)
1	Prof. R. Jones, Dept. of Civil Eng., Ohio State University, 206 W 18th Avenue, Columbus, Ohio 43210
1	State University of New York at Stony Brook, Stony Brook, New York 11790 ATTN: Prof. Fu-Pen Chiang, Dept. of Mechanics
1	E. I. Du Pont de Nemours and Company, Wilmington, Delaware 19898 ATTN: Dr. Carl Zweren, Industrial Fibers Div., Textile Fibers Department
1	Washington University, St. Louis, Missouri 63130 ATTN: Prof. E. M. Wu
	Director, Army Materials and Mechanics Research Center, Watertown, Massachusetts 02172
2	ATTN: DRXMR-PL
1	DRXMR-AP
1	DRXMR-X
1	DRXMR-XP
1	DRXMR-CT
1	DRXMR-T
1	DRXMR-TM, Dr. Leroe
47	DRXMR-TM, Mr Uplinger
1	Author

AD ————————————
UNCLASSIFIED
UNLIMITED DISTRIBUTION

Army Materials and Mechanics Research Center,
Watertown, Massachusetts 02172
STRUCTURAL ANALYSIS AND TESTING
FOR COMPOSITE FLYWHEEL DEVELOPMENT
Donald E. Johnson
Avco Systems Division
201 Lowell St., Wilmington, MA 01887
Final Report Contract Number DAAG46-77-C0017
illus - tables, Contract DAAG46-77-C-0017
Final Report, January 24, 1977 to September 3, 1977

Key Words

Flywheels
Composite materials
Failure
Fracture
Stress analysis

Several effects that can limit the performance of bi-directionally reinforced composite fly-
wheels are investigated. These effects include potential shear failures, degraded properties and
variations caused by manufacturing. Finite element analyses are used to determine both the
in-plane and interlaminar shear stresses that arise from the discreteness of the individual radial
reinforcements. The degradation of material properties due to high biaxial stress levels, es-
pecially a drop in shear modulus, is also investigated. Degraded properties are obtained experi-
mentally and used in the evaluation of flywheel performance. Also included is an analysis to
determine the feasibility of a static simulation test. In addition, the effect of asymmetric
material property variation on flywheel imbalance was investigated.

AD ————————————
UNCLASSIFIED
UNLIMITED DISTRIBUTION

Army Materials and Mechanics Research Center,
Watertown, Massachusetts 02172
STRUCTURAL ANALYSIS AND TESTING
FOR COMPOSITE FLYWHEEL DEVELOPMENT
Donald E. Johnson
Avco Systems Division
201 Lowell St., Wilmington, MA 01887
Final Report Contract Number DAAG46-77-C0017
illus - tables, Contract DAAG46-77-C-0017
Final Report, January 24, 1977 to September 3, 1977

Key Words

Flywheels
Composite materials
Failure
Fracture
Stress analysis

Several effects that can limit the performance of bi-directionally reinforced composite fly-
wheels are investigated. These effects include potential shear failures, degraded properties and
variations caused by manufacturing. Finite element analyses are used to determine both the
in-plane and interlaminar shear stresses that arise from the discreteness of the individual radial
reinforcements. The degradation of material properties due to high biaxial stress levels, es-
pecially a drop in shear modulus, is also investigated. Degraded properties are obtained experi-
mentally and used in the evaluation of flywheel performance. Also included is an analysis to
determine the feasibility of a static simulation test. In addition, the effect of asymmetric
material property variation on flywheel imbalance was investigated.

AD ————————————
UNCLASSIFIED
UNLIMITED DISTRIBUTION

Army Materials and Mechanics Research Center,
Watertown, Massachusetts 02172
STRUCTURAL ANALYSIS AND TESTING
FOR COMPOSITE FLYWHEEL DEVELOPMENT
Donald E. Johnson
Avco Systems Division
201 Lowell St., Wilmington, MA 01887
Final Report Contract Number DAAG46-77-C0017
illus - tables, Contract DAAG46-77-C-0017
Final Report, January 24, 1977 to September 3, 1977

Key Words

Flywheels
Composite materials
Failure
Fracture
Stress analysis

Several effects that can limit the performance of bi-directionally reinforced composite fly-
wheels are investigated. These effects include potential shear failures, degraded properties and
variations caused by manufacturing. Finite element analyses are used to determine both the
in-plane and interlaminar shear stresses that arise from the discreteness of the individual radial
reinforcements. The degradation of material properties due to high biaxial stress levels, es-
pecially a drop in shear modulus, is also investigated. Degraded properties are obtained experi-
mentally and used in the evaluation of flywheel performance. Also included is an analysis to
determine the feasibility of a static simulation test. In addition, the effect of asymmetric
material property variation on flywheel imbalance was investigated.

AD ————————————
UNCLASSIFIED
UNLIMITED DISTRIBUTION

Army Materials and Mechanics Research Center,
Watertown, Massachusetts 02172
STRUCTURAL ANALYSIS AND TESTING
FOR COMPOSITE FLYWHEEL DEVELOPMENT
Donald E. Johnson
Avco Systems Division
201 Lowell St., Wilmington, MA 01887
Final Report Contract Number DAAG46-77-C0017
illus - tables, Contract DAAG46-77-C-0017
Final Report, January 24, 1977 to September 3, 1977

Key Words

Flywheels
Composite materials
Failure
Fracture
Stress analysis

Several effects that can limit the performance of bi-directionally reinforced composite fly-
wheels are investigated. These effects include potential shear failures, degraded properties and
variations caused by manufacturing. Finite element analyses are used to determine both the
in-plane and interlaminar shear stresses that arise from the discreteness of the individual radial
reinforcements. The degradation of material properties due to high biaxial stress levels, es-
pecially a drop in shear modulus, is also investigated. Degraded properties are obtained experi-
mentally and used in the evaluation of flywheel performance. Also included is an analysis to
determine the feasibility of a static simulation test. In addition, the effect of asymmetric
material property variation on flywheel imbalance was investigated.